



HAL
open science

Behavior of calcined clay based geopolymers under sulfuric acid attack: Meta-illite and metakaolin

Laura Diaz Caselles, Bastien Balsamo, Virginie Benavent, Vincent Trincal, Hugo Lahalle, Cédric Patapy, Valérie Montouillout, Martin Cyr

► To cite this version:

Laura Diaz Caselles, Bastien Balsamo, Virginie Benavent, Vincent Trincal, Hugo Lahalle, et al.. Behavior of calcined clay based geopolymers under sulfuric acid attack: Meta-illite and metakaolin. Construction and Building Materials, 2023, 363, pp.129889. 10.1016/j.conbuildmat.2022.129889 . hal-04032808

HAL Id: hal-04032808

<https://hal.science/hal-04032808>

Submitted on 16 Mar 2023

HAL is a multi-disciplinary open access archive for the deposit and dissemination of scientific research documents, whether they are published or not. The documents may come from teaching and research institutions in France or abroad, or from public or private research centers.

L'archive ouverte pluridisciplinaire **HAL**, est destinée au dépôt et à la diffusion de documents scientifiques de niveau recherche, publiés ou non, émanant des établissements d'enseignement et de recherche français ou étrangers, des laboratoires publics ou privés.

1 **Behavior of calcined clay based geopolymers under sulfuric acid attack: Meta-illite and**
2 **metakaolin** Laura Diaz Caselles^{a,*}, Bastien Balsamo^a, Virginie Benavent^a, Vincent Trincal^a, Hugo
3 LaHalle^a, Cédric Patapy^a, Valérie Montouillout^b, Martin Cyr^a

4
5 ^a LMDC, INSA/UPS Génie Civil, 135 Avenue de Rangueil, 31077 Toulouse cedex 04 France.

6 ^b CNRS, CEMHTI UPR3079, Univ. Orléans, F-45071 Orléans, France

7 *Corresponding author: diazcase@insa-toulouse.fr

8 **Abstract**

9 Durability of geopolymers in aggressive environments are encouraging but deeper investigations are
10 needed to understand the acid resistance of calcined clay geopolymers. This paper compares the behavior
11 of four different calcined clay-based geopolymers under sulfuric acid attack and gives insights into the
12 degradation mechanisms of meta-illite based geopolymers, which had not been addressed in the literature
13 until now. Paste samples were cast using metakaolin and meta-illite as the precursors and were activated
14 by either sodium silicate or potassium silicate solutions. After curing, geopolymers pastes were
15 submerged in sulfuric acid solution at pH 1 for 30 days. Mineralogical, microscopic, and chemical
16 analyses indicated that geopolymer pastes were affected by leaching of alkali cations into the immersion
17 solution, and thus by a disequilibrium of the geopolymer network. Among all materials, meta-illite based
18 geopolymers activated by sodium silicate presented the least damage and hold promise for improving the
19 durability of materials under sulfuric acid attack.

20
21 **Keywords:** geopolymerization, durability, alkali activated material, sulfuric acid attack, calcined clay,
22 sodium silicate, potassium silicate

24 1. Introduction

25 Concrete structures may be susceptible to bio-deterioration in wastewater networks and other
26 fermentation or methanogenesis environments due to complex mechanisms of sulfate/acid attacks. For
27 instance, the so-called Microbially Induced Corrosion of Concrete (MICC) in sewer environments is a
28 multi-step process occurring in the presence of anaerobic bacteria that reduce sulfate ions (SO_4^{2-}) into
29 hydrogen sulfide (H_2S) [1–3]. Solutions containing H_2S present very low pH values (e.g., pH 1 and pH 3),
30 which, on conventional concrete, lead to a decrease in pH of the material surface (around 9) [4–9]. This
31 condition and the presence of sulfur develop a suitable environment for sulfur-oxidizing bacteria, which
32 oxidize the reduced sulfur into H^+ and SO_4^{2-} [10,11]. Ordinary Portland Cement (OPC) has shown poor
33 performance under sulfuric acid attack due to the leaching of Ca-rich phases and the formation of
34 expansive products such as gypsum ($\text{CaSO}_4 \cdot 2\text{H}_2\text{O}$) leading to material loss [3,12]. Therefore, it is
35 necessary to improve the durability of construction materials under sulfuric acid environments.
36 Preliminary investigations carried out on geopolymers (Ca-poor materials) in aggressive environments are
37 encouraging, especially for fly-ash based geopolymers [13–18]. However, deeper investigations are
38 needed to understand the acid resistance of calcined clay geopolymers.

39 Geopolymers are alternative materials to OPC and are made by mixing solid powders that are sources
40 (precursors) of aluminosilicates (e.g., calcined clays, fly ashes) with alkaline activating solutions (alkali
41 silicate-based or alkali hydroxide-based such as sodium (Na) or potassium (K) based activators, for
42 example) [19–21]. The reaction produced between the precursors and the alkaline solution is referred to
43 as “geopolymerization”. Clay minerals (phyllosilicates) are natural aluminosilicate resources, in which
44 silicon (Si) is in 4-fold coordination, while aluminum (Al) is in 4-, 5- or 6-fold coordination [22–24].
45 After calcination, Al coordination changes from 6-fold to 4-fold and the precursor becomes amorphous
46 (loss of crystallinity), which enables its dissolution in the alkaline solution [23]. After geopolymerization,
47 a three-dimensional synthetic material is obtained and is referred to as “Si-O-Al-O network”, where Si
48 and Al are both in 4-fold coordination [19,25]. The charge in the geopolymer network is balanced by the

49 alkali cations (K^+ and Na^+) [25]. In these materials, water is found in several states: slightly confined
50 water in the porosity, physically bound water at the pore surface, and water in the hydration sphere of
51 alkali cations [26].

52 Among the different clay minerals studied in the literature, kaolinite has been very popular for its
53 potential as a precursor in alkali activated materials [24]. Gao et al., 2013 [27] studied a metakaolin (MK)
54 geopolymer activated by K-silicate under hydrochloric acid (HCl) at pH 2 and showed that the
55 geopolymer network was relatively stable during the first 28 days of testing. Up to this point, little
56 damage was attributed to the exchange of K^+ with H^+ ions in the solution, which increased the number of
57 Si-OH and Al-OH groups in the geopolymer. Similarly, Bouguermouh et al., 2017 [28] reported that MK-
58 based geopolymers activated either by K-silicate or by Na-silicate showed good resistance to HCl.
59 Conversely, Vogt et al., 2020 [29] showed that MK-based geopolymer activated by K-silicate presented
60 degradation after sulfuric acid attack, due to the release of K^+ into solution, followed by the
61 dealumination and depolymerization of the geopolymer. Similarly, Grengg et al., 2021 [30] studied a low-
62 Ca MK-based geopolymer (CaO = 2.5 wt.%) activated by K-silicate with addition of Cu under sulfuric
63 acid attack at pH 2. The authors indicated that, after 35 days of exposure, the material presented complete
64 dissolution of the geopolymer framework and the precipitation of expansive sulfate phases.

65 As previously exposed, the literature about acid resistance of calcined clay geopolymers mainly focuses
66 on metakaolin (calcined kaolinite) based systems [27,29,31] and data on the acid resistance of other
67 calcined clay based geopolymers is practically inexistent. Nonetheless, other common calcined clays (i.e.,
68 meta-illite) have been studied in the literature as Portland cement replacements due to their potential
69 pozzolanic activity, low cost, abundant availability, and low CO_2 emission in addition to their good
70 mechanical performance [32]. Therefore, the present publication focuses on the study of two calcined
71 clays: metakaolin (MK) and meta-illite (MI) used as precursors for the fabrication of geopolymers. These
72 two calcined clays belong to the two main groups of clay minerals, referred to as 1:1 and 2:1 minerals,
73 respectively [22,33]. These ratios refer to the crystallographic structures of the clay minerals, which

74 consist of regular repetition of tetrahedral and octahedral sheets. Tetrahedral sheets are usually Si^{4+} or
75 Al^{3+} (each cation surrounded by four oxygens) and octahedral sheets are either divalent cations (Mg^{2+} ,
76 Fe^{2+}) or trivalent cations (Al^{3+} , Fe^{3+}) [22,24,33]. This paper aims to (i) compare the resistance of MK and
77 MI based geopolymers under sulfuric acid (H_2SO_4) attack, and (ii) gain insights into their degradation
78 mechanisms. Four different geopolymer pastes were cast using MK and MI precursors and were activated
79 by two different alkaline solutions (Na-silicate and K-silicate). Sulfuric acid attack of geopolymers was
80 performed under highly aggressive conditions by submerging 28 day cured paste samples in an H_2SO_4
81 solution at pH 1 for 30 days. The resistance of the geopolymers to sulfuric acid was assessed by direct
82 observations and by measuring the mass change of samples over time. To understand the degradation
83 mechanisms, the chemical composition of the immersion solutions was determined, and mineralogical
84 and microscopic characterizations were performed on the geopolymers before and after sulfuric acid
85 attack.

86 **2. Materials and Methods**

87 **2.1. Materials**

88 **2.1.1. Binders/precursors**

89 The chemical compositions of the calcined clays (precursors) and the reference binder (ordinary Portland
90 cement) were obtained by X-ray fluorescence and are presented in Table 1. The precursors/binders tested
91 were:

- 92 - Ordinary Portland cement (CEM I), CEM I 52.5 N CE CP2 NF, from LAFARGE. This cement has
93 a specific gravity of 3.15 g/cm^3 and a Blaine specific surface of $4160 \text{ cm}^2/\text{g}$. It was used as the
94 reference binder.
- 95 - Metakaolin (MK) manufactured at Fumel by ARGECO, with a specific gravity of 2.59 g/cm^3 and a
96 BET specific surface area of $17 \text{ m}^2/\text{g}$.

97 - Meta-illite (MI) manufactured by VICAT, with a specific gravity of 2.59 g/cm³ and a BET specific
 98 surface area of 20 m²/g.

99 **Table 1** Chemical compositions of the binder/precursors, obtained by X-ray fluorescence (% by weight).

	CaO	SiO ₂	Al ₂ O ₃	Fe ₂ O ₃	MgO	MnO	Na ₂ O	K ₂ O	SO ₃	TiO ₂	LOI*
CEM I	65.5	20.6	4.3	2.4	0.7	0.1	0.1	0.2	3.1	0.2	2.7
MK	0.7	68.2	23.4	3.6	1.2	0.0	0.2	0.2	0.0	1.2	1.2
MI	4.4	52.7	25.5	7.0	3.5	0.1	0.3	2.9	0.0	1.0	2.6

100 *Loss on ignition, T= 1000°C

101
 102 The mineralogical compositions of MK and MI precursors are presented in Table 2 and were obtained by
 103 XRD Rietveld analyses following the parameters described in Trincal et al., 2014 [34] and previously
 104 published in Lahalle et al., 2021 [35].

105 **Table 2** Mineralogical composition of the metakaolin (MK) and meta-illite (MI) estimated by XRD Rietveld
 106 analyses (% by weight).

	Amorphous	Quartz	Illite	Mullite	Anatase	Calcite	Hematite	Rutile
MK	47.1±2.5	42.3±1.6	3.5±0.5	3.1±0.4	1.5±0.1	1±0.1	0.9±0.1	0.3±0.1
MI	61.3±7.9	13.5±2.3	19.0±6.7	-	-	2.6±1.6	2.0±1.4	1.7±1.7

107 2.1.2. Activators

108 MK and MI were activated by two different commercial products:

109 - Na-silicate solution with an SiO₂/Na₂O molar ratio of 1.7, specific gravity of 1.55 g/cm³ at 20 °C
 110 (Betol[®] 47T: 27.5% SiO₂, 16.9% Na₂O and 55.6% H₂O, % by weight).

111 - K-silicate solution with an SiO₂/K₂O molar ratio of 1.7, specific gravity of 1.5 g/cm³ at 20 °C
 112 (Geosil[®] 14517: 24% SiO₂, 21% K₂O and 55% H₂O, % by weight).

113 2.1.3. Sample preparation and curing

114 MK-based geopolymer pastes activated either by Na-silicate or by K-silicate are referred to as “MK_Na”
 115 and “MK_K”, respectively. MI-based geopolymer pastes activated either by Na-silicate or by K-silicate
 116 are referred to as “MI_Na” and “MI_K”, respectively. For all the geopolymer pastes, the water content of
 117 the commercial solutions was adjusted to obtain a water to solid (w/s) ratio of 0.4. “Solid” consisted of
 118 the total amount of calcined clay and the dry part of the activating solution (SiO₂, Na₂O and K₂O).

- 119 • MK_Na and MI_Na: MK and MI precursors were activated by adding Na-silicate solution at
 120 77 wt. % and 78.9 wt. %, respectively (% by weight of precursor).
- 121 • MK_K and MI_K geopolymers: MK and MI precursors were activated by adding K-silicate
 122 solution at 78 wt. % and 78.2 wt. %, respectively.

123 The amorphous and quartz contents were different in the two precursors (MK and MI). Thus, the amount
 124 of reactive binder varied since only the amorphous part of calcined clays is considered to react during the
 125 alkali activation process. To avoid misleading conclusions, CEM I and MI geopolymer pastes were
 126 prepared using the same quartz content as in MK precursor. Therefore, a content of 50 wt. % quartz was
 127 targeted for all the formulations (crushed sand < 120 μm). It should be noted that samples prepared in this
 128 study were all pastes containing equivalent quartz amounts and they should not be confused with mortars.

129 All pastes were prepared following the recommendations of European Standard NF EN 196-3 and using a
 130 hand held electric mixer as described in Lahalle et al., 2021 [35]. Pastes were cast into hermetic,
 131 cylindrical PVC molds 6 cm in length and 3 cm in diameter and stored for 28 days in a room at T=20 °C,
 132 RH=50% until characterization and acid immersion. The mix design of all the geopolymer pastes is
 133 presented in Table 3.

134 **Table 3** Mix design of all the geopolymer pastes.

CEM I (g)	MK (g)	MI (g)	Quartz ^a (g)	Activator ^b (g)	Water activator ^c (g)	Dry activator ^d (g)	Added water ^e (g)	w/s ^f
-----------	--------	--------	----------------------------	-------------------------------	--	--------------------------------------	------------------------------------	------------------

CEM I	250	-	-	250	-	-	-	400	0.4
MK_Na	-	500	-	-	385 ^g	213	171	51	0.4
MK_K	-	500	-	-	390 ^h	216	174	55	0.4
MI_Na	-	-	289	211	228 ^g	127	101	114	0.4
MI_K	-	-	289	211	226 ^h	125	100	116	0.4

135 ^a Total amount of quartz added to the mixture, which is equivalent to the quartz content present in the MK
136 precursor.

137 ^b Total amount of the activator.

138 ^c Water coming from the activator.

139 ^d Dry part coming from the activator.

140 ^e Supplementary added water.

141 ^f Effective water content to solid ratio (solid: anhydrous binder + sand + dry activator).

142 ^f Na-silicate

143 ^g K-silicate

144 2.2. Methods

145 2.2.1. Sulfuric acid attack test

146 After curing, all paste samples were kept into the original plastic molds for the sulfuric acid tests. In order
147 to cause unidirectional attack, only the top of the samples was exposed. The top borders of the plastic
148 molds (i.e., edges) were protected/sealed with a commercial epoxy resin (Resoltech 3030 BLANC) to
149 avoid penetration of the solution into the recipient. Twenty-four hours after application of the resin, five
150 samples per formulation were taken for sulfuric acid tests. First, all samples were weighed and then,
151 submerged in a sulfuric acid (H₂SO₄) solution prepared with distilled water and having a pH of 1±0.3.
152 Paste samples were not previously saturated before sulfuric acid attack to avoid disequilibrium in the pore
153 solution of geopolymers and thus, to avoid misleading conclusions [36]. The H₂SO₄ solution was stored
154 in closed individual plastic buckets keeping a liquid to solid (L/S) ratio of 20 (i.e., 3.7 litres of solution
155 per bucket and per formulation) and stored in a room at T=20 °C. Direct observations and mass change
156 measurements were made over time for a total of 30 days (results are presented for 1, 5, 12, 20 and 30
157 days). Values are presented as the arithmetic mean of all results, with a confidence interval of 95%.

158 Moreover, the pH of the solutions was manually monitored over time using a digital pH meter. Since pH
159 was stable at 1±0.3, solutions were not renewed during the test. Major element concentrations were
160 determined in the immersion solutions by Inductively Coupled Plasma Atomic Emission Spectrometry

161 (ICP-AES using a Perkin Elmer Optima 7000 DV) after 4 hours of immersion (referred to as 0.17 d) and
162 at 2, 5, 20, and 30 days of testing. All solution samples were diluted by a factor of 25 using ultrapure
163 water (18.2 MΩ.cm) at 2 % nitric acid (HNO₃) (v/v). Sulfate concentrations were determined by ion
164 chromatography (Dionex Ion Chromatography System ICS-3000) and solutions were diluted by a factor
165 of 250 using ultrapure water (18.2 MΩ.cm). Two solution samples were analyzed per formulation and
166 arithmetic mean values were calculated with a confidence interval of 95%.

167 **2.2.2. SEM/EDS analyses**

168 Scanning electron microscope (SEM) observations were performed on carbon-coated calcined clays and
169 polished sections of geopolymer pastes previously mounted in resin. Two different scanning electron
170 microscopes were used, a JEOL JSM-6380LV and a JEOL JSM 7800, equipped with
171 Rontec XFLASH 3001 and SDD X-Max 80 mm² electron dispersive spectroscopy (EDS) detectors,
172 respectively. A series of 10 images and about 300 EDS points were taken per sample during the analyses.
173 Images were obtained in both secondary electron (SE) and backscattered electron (BSE) configuration,
174 applying magnifications between 25x and 100,000x. EDS mappings were obtained over a relatively large
175 area (5000 x 3000 μm) by applying a low magnification of 25x and covering the transition zones between
176 the unaltered and altered zones of geopolymers after sulfuric acid attack.

177 **2.2.3. XRD, FT-IR and MAS NMR analyses**

178 All samples, geopolymer pastes before and after (altered layer of the geopolymers) sulfuric acid attack,
179 were crushed manually in an agate mortar to a particle size below 80 μm (sieve control) and dried in an
180 oven at 40 °C to remove the free water. Then, all samples were investigated by X-ray diffraction (XRD),
181 Fourier-Transform Infrared Spectroscopy (FT-IR) and solid-state magic-angle spinning nuclear magnetic
182 resonance (MAS NMR) analyses.

183 XRD analyses were performed by using a Bruker D8 diffractometer in Bragg-Brentano configuration
184 with a copper radiation source (Cu K α , $\lambda=1.54 \text{ \AA}$). The diffractometer was equipped with a vertical theta /
185 theta goniometer, a LynxEye XE-TTM high-speed linear detector and a motorized anti-scattering knife.
186 The anticathode voltage was 40 kV, and the electric current intensity was 40 mA. 2θ angles from 5° to
187 70° were scanned with a 2θ step size of 0.02° and a total scan duration of 2.5 hours. Minerals were
188 identified using the Bruker-AXS DIFFRACplus Eva v4 software and the 2015 ICDD PDF database.

189 FT-IR analyses were performed to detect structural modifications on absorption bands present in the
190 geopolymers. Analyses were performed using a Perkin Elmer UATR1 device with a diamond crystal.
191 Data were collected over the wavenumber range of $4000\text{-}600 \text{ cm}^{-1}$. Finally, environmental changes in Al
192 and Si geopolymer networks were studied by solid state MAS NMR. ^{27}Al spectra were acquired on a
193 Bruker AVANCE III spectrometer operating at 221 MHz ($B_0 = 20 \text{ T}$) with a spinning speed of 30 kHz
194 (2.5 mm zirconia rotors). 1D MAS spectra were acquired after a single short pulse ($\pi/10$) ensuring a
195 quantitative excitation and quantification of ^{27}Al central transition and 3072 scans were accumulated with
196 a recycling delay of 1 s. ^{29}Si spectra were acquired on a Bruker AVANCE I spectrometer operating at
197 79 MHz ($B_0 = 9.4 \text{ T}$) with a spinning speed of 6 kHz (7 mm zirconia rotors). Around 2000 scans were
198 accumulated with a recycling delay of 60 s ensuring the complete relaxation of the signal except for those
199 of quartz. Chemical shifts were referenced to $(\text{Al}(\text{NO}_3)_3)$ and (TMS) for ^{27}Al and ^{29}Si MAS NMR
200 analyses, respectively. For ^{27}Al MAS NMR analyses, results are presented in terms of Al(IV), Al(V) and
201 Al(VI), which refer to the coordination numbers. For ^{29}Si NMR results, coordination numbers are referred
202 to as Q_n , where the subscript number indicates the number of bonding oxygens. ^{27}Al and ^{29}Si MAS NMR
203 spectra were processed using the Dmfit program developed at CEMHTI [37].

204 **2.2.4. Mercury intrusion porosimetry (MIP)**

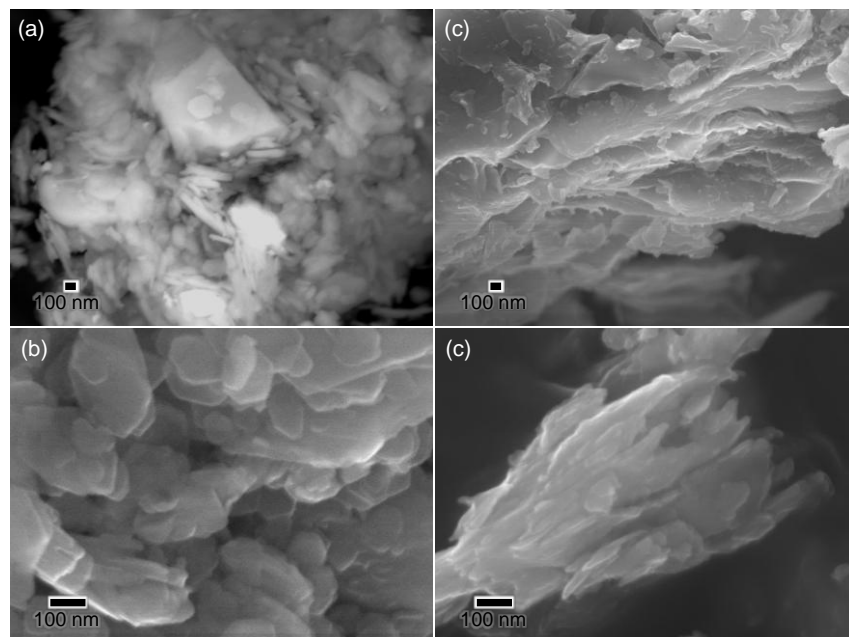
205 Geopolymers pastes, before sulfuric acid attack, were investigated by MIP (AutoPore IV 9500
206 Porosimeter from Micromeritics according to the standard ISO 15901-1 2005) in order to obtain

207 information on their total porosity accessible to mercury and their pore size distribution. The mercury
208 pressure used varied from 0.0007 MPa to 400 MPa and information was obtained on pore access
209 diameters greater than 3 nm. Geopolymer pastes of about 1 g to 3 g were analyzed per formulation and
210 were not dried before the test but put directly into the penetrometer, which allowed to the dehydration of
211 samples during the evacuation process in the porosimeter as described by Trincal et al., 2022 [38]. Only
212 one test was carried out per type of material.

213 3. Results

214 3.1. Characterization of samples before sulfuric acid attack

215 The morphology of calcined clays was characterized by SEM observations before geopolymerization. Fig.
216 1 shows SE images obtained from MK and MI precursors, revealing that microstructures of the two
217 calcined clays were different. MK presented massive hexagonal flat platelets with lengths of the order of
218 100-200 nm (cf. Fig. 1a and b). In contrast, MI grain particles displayed an agglomerate of numerous
219 layers with variable, irregular shapes (cf. Fig. 1c and d).



220

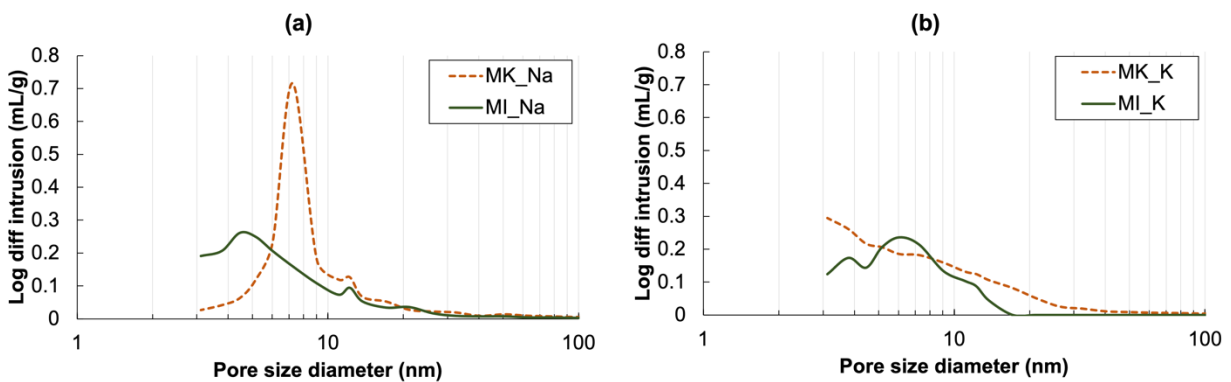
221 **Fig. 1.** SE images obtained from particles of calcined clays (a), (b) metakaolin (MK), and (c), (d) meta-illite (MI).

222 Table 4 gives information on the total volume of mercury intruded for estimation of the total accessible
 223 porosity, and Fig. 2 presents the pore size distribution determined in unaltered geopolymers at 28 days of
 224 curing.

225 **Table 4** Total intruded volume of mercury in unaltered pastes, determined by MIP.

Unaltered geopolymer	CEM I	MK_Na	MK_K	MI_Na	MI_K
Total intruded volume (%)	35.2	29.8	30.5	26.5	30.8

226



227

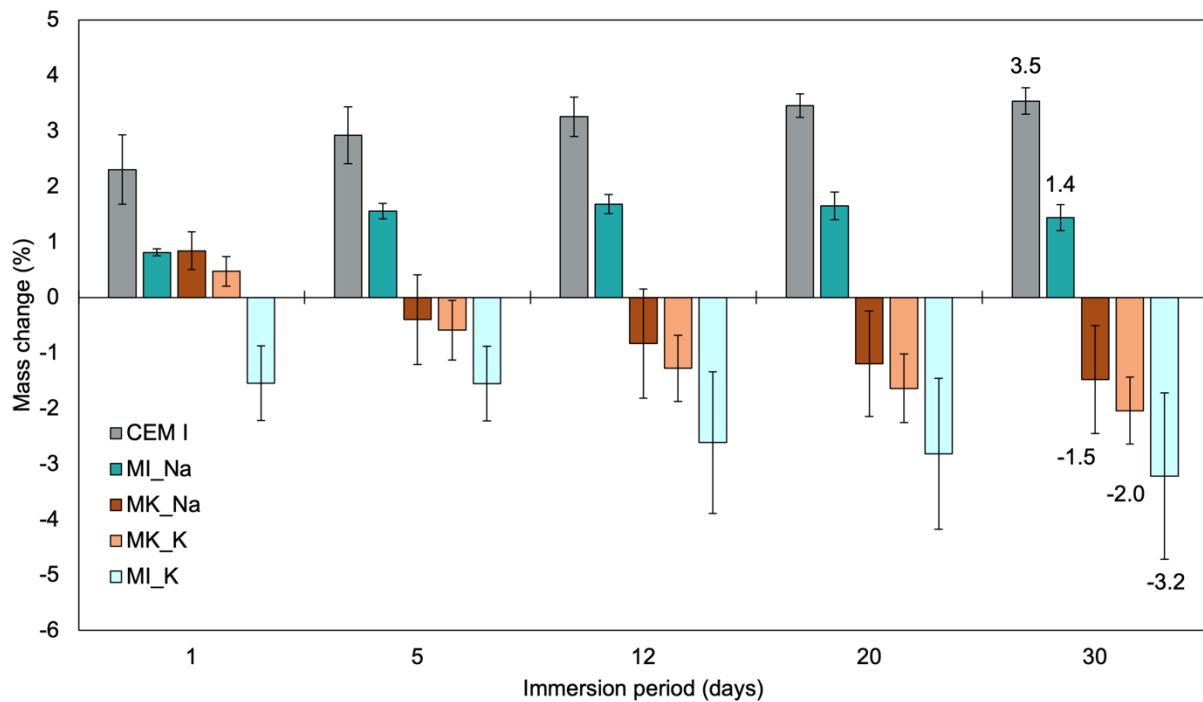
228 **Fig. 2.** Pore size distribution obtained by MIP for unaltered geopolymers. (a) MK_Na and MI_Na, (b) MK_K and
 229 MI_K.

230 The results presented in Table 4 and Fig. 2 indicate that geopolymers activated by K-silicate seemed to
 231 present higher values of total accessible porosity than those activated by Na-silicate. MI_Na geopolymer
 232 presented the least total accessible porosity among all geopolymers. Moreover, geopolymers activated by
 233 Na-silicate exhibited a pore mode, which is in line with observations found in the literature [39,40].
 234 MK_Na and MI_Na geopolymers presented one main population of pore sizes, placed at 7.2 nm and
 235 4.5 nm, respectively. In contrast, MK_K geopolymers presented a large range of pore sizes mainly

236 smaller than 20 nm, and MI_K presented a main population of pore size at 6 nm. Results indicate the
 237 existence of pore sizes smaller than 3 nm, which were not measured by this method.

238 **3.2. Mass change and direct observations during sulfuric acid attack**

239 Fig. 3 presents the mass change measured over time for CEM I and geopolymer pastes exposed to sulfuric
 240 acid attack. Table 5 presents the pH evolution measured in the immersion solution over time and Fig. 4
 241 presents the images obtained from the cross-sectional view of all geopolymers, using an optical
 242 microscope to evaluate the appearance of the exposed surfaces after sulfuric acid attack.



243

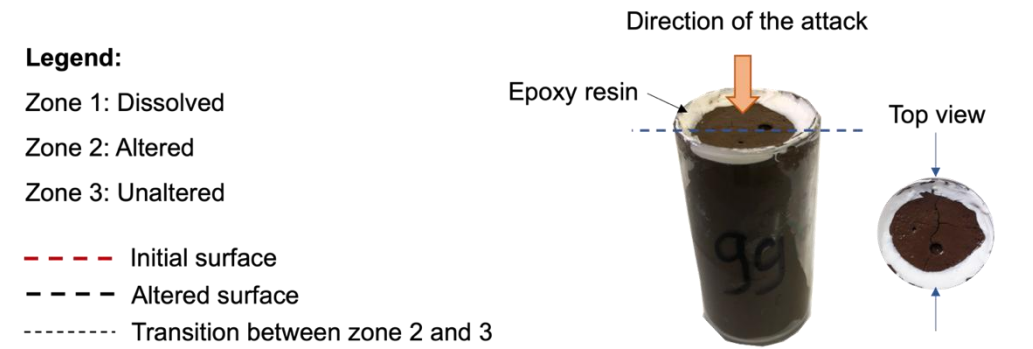
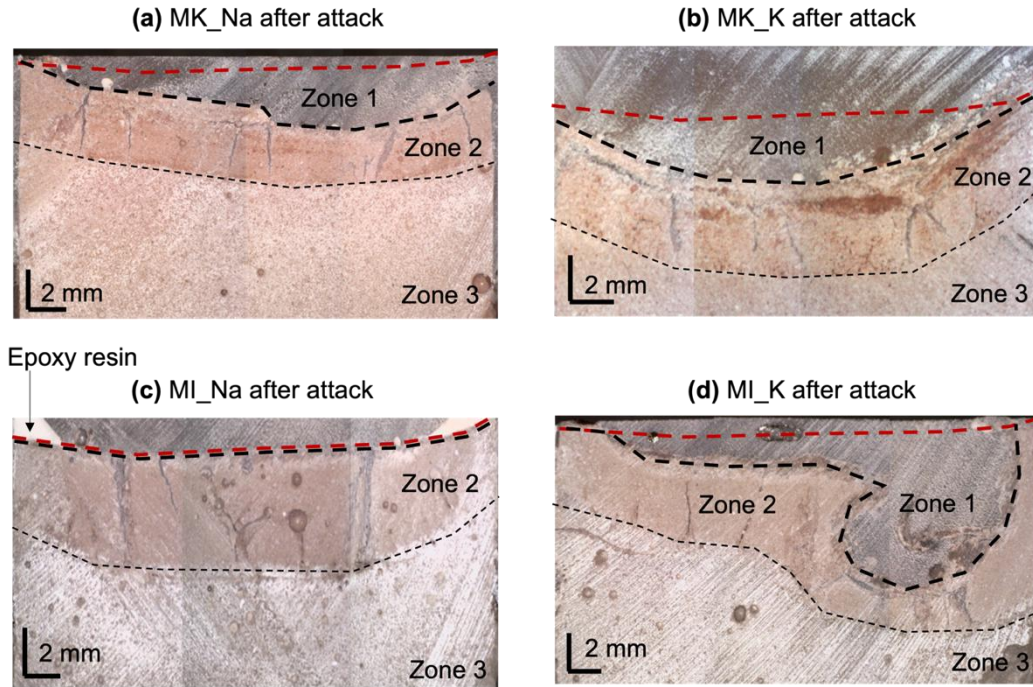
244 **Fig. 3.** Mass change given in percentage, versus immersion period in days for pastes under sulfuric acid attack at pH
 245 1. Values are presented as the average of five results, with a confidence interval of 95%.

246 **Table 5** Evolution of pH in the sulfuric acid (H₂SO₄) immersion solutions of pastes. The pH of the solutions was
 247 manually monitored over time using a digital pH meter. pH was considered stable at 1±0.3.

Immersion solution/Time (d)	0	1	5	12	20	30
-----------------------------	---	---	---	----	----	----

CEM I	1.21	1.08	1.09	1.11	1.18	1.08
MI_Na	1.20	1.16	1.12	1.13	1.21	1.16
MK_Na	1.14	1.13	1.13	1.21	1.30	1.27
MK_K	1.20	1.10	1.17	1.24	1.27	1.16
MI_K	1.16	1.08	1.13	1.19	1.21	1.24

Optical microscope images – Cross section view

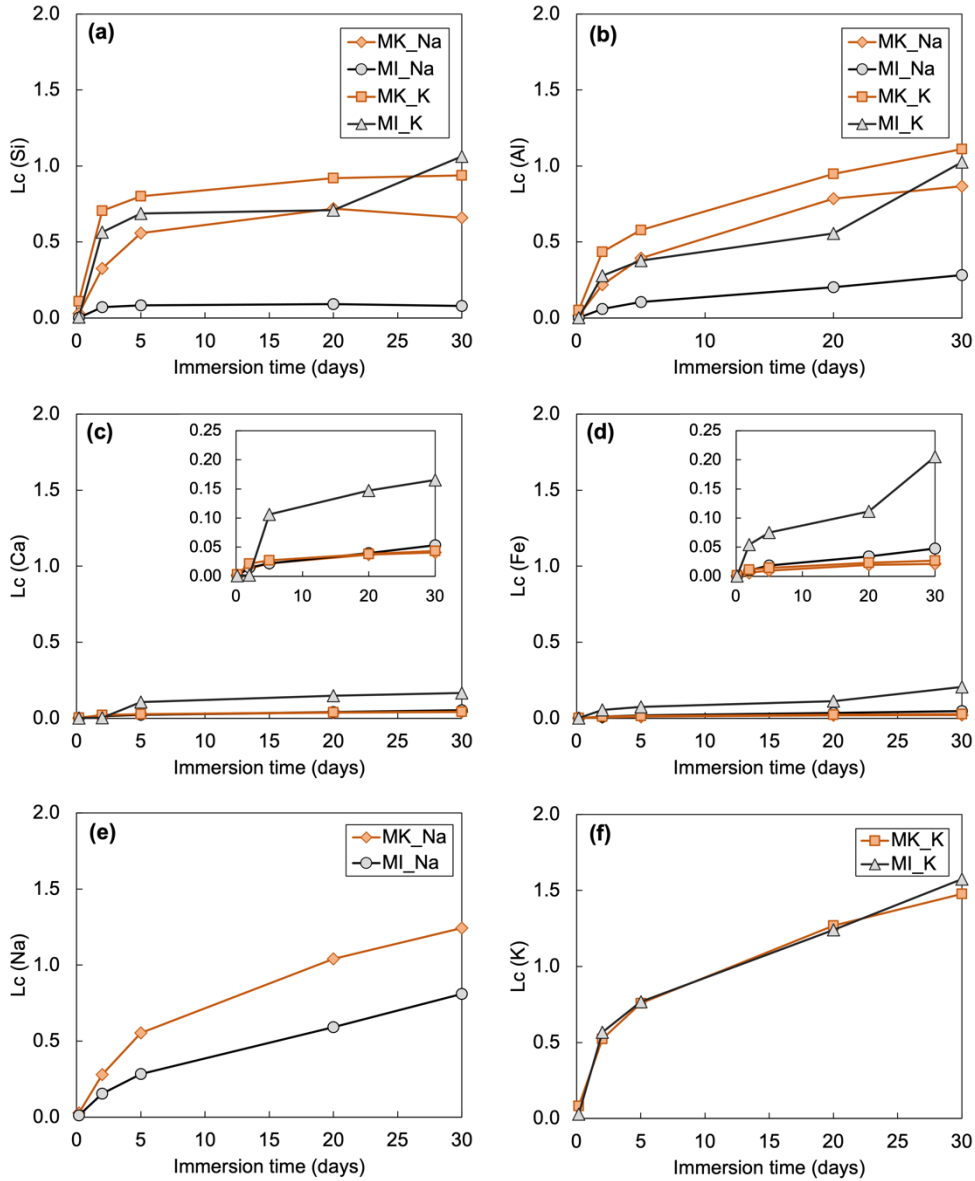


250 **Fig. 4.** Optical microscope images (cross sectional view) of attacked geopolymers. Zone 1: dissolved material, zone
 251 2: altered geopolymer, and zone 3: unaltered geopolymer. (a) MK_Na, (b) MK_K, (c) MI_Na, and (d) MI_K.

252 As observed in Fig. 3, all samples (except MI_K) presented a gain in mass on the first day of immersion,
253 which was attributed to the uptake of water. At the end of the test (at 30 days), CEM I pastes presented a
254 gain in mass of $3.5\% \pm 0.2\%$, followed by the MI_Na geopolymer, in which a gain in mass of $1.4\% \pm 0.2\%$
255 was obtained. In contrast, MK_Na, MK_K and MI_K geopolymers presented mass losses of $1.5\% \pm 0.9\%$,
256 $2.0\% \pm 0.6\%$ and $3.2\% \pm 1.5\%$, respectively. Furthermore, direct observations of the geopolymer cross-
257 sections (cf. Fig. 4) allowed the altered (or corrosion) depth layer to be estimated in all the samples. Three
258 distinct zones were identified: (i) dissolved material, (ii) altered geopolymer (characterized by a layer
259 about 4-5 mm deep, with microcracks), and (iii) unaltered or non-attacked geopolymer. Fig. 4a and b
260 show that exposed surfaces of MK_Na and MK_K geopolymers were altered and about 2-4 mm of
261 material had been dissolved at the end of the test. In the case of MI-based geopolymers, MI_K seemed to
262 be the most altered material, exhibiting a considerable loss of material (cf. Fig. 4d). Meanwhile, MI_Na
263 geopolymer presented an exposed surface that was not visibly dissolved even though several vertical
264 microcracks were identified (cf. Fig. 4c).

265 **3.3. Chemical evolution of the immersion solution**

266 Fig. 5 presents the evolution of the leaching coefficient (Lc) according to time. Fig. 5 allows to compare
267 the degree of leaching of the geopolymer pastes (MK_Na, MK_K, MI_Na and MI_K). In the present
268 paper, the leaching coefficients were calculated according to [41,42] and considering the total volume of
269 samples submerged in the sulfuric acid solution and thus, the initial molar concentrations of Si, Al, Ca,
270 Fe, Na, K, Mg and Ti present in the solid fraction of the geopolymers (cf. Table 1) as well as the
271 additional Si, K, and Na amount coming from the activators (cf. Table 3). A Lc equal to 0 means that the
272 element was not leached from the geopolymers, and a Lc equal to 100 indicates that the element was
273 completely leached.



274

275 **Fig. 5.** Evolution of the leaching coefficients (Lc) determined according to time for MK_Na, MK_Na, MI_K and
 276 MI_K geopolymers during the sulfuric acid attack. **(a)** Silicon, **(b)** Aluminum, **(c)** Calcium, **(d)** Iron, **(e)** Sodium,
 277 and **(f)** Potassium.

278 As observed in Fig. 5, the degree of leaching increased over time for all the samples. Overall, the rate of
 279 Si release into the immersion solution was characterized by an accelerated rate during the first five days.
 280 After this point, Si concentrations were relatively stable, except for the immersion solution of MI_K
 281 geopolymer, in which the concentration of Si increased at the end of the test (cf. Fig. 5a). Regarding the

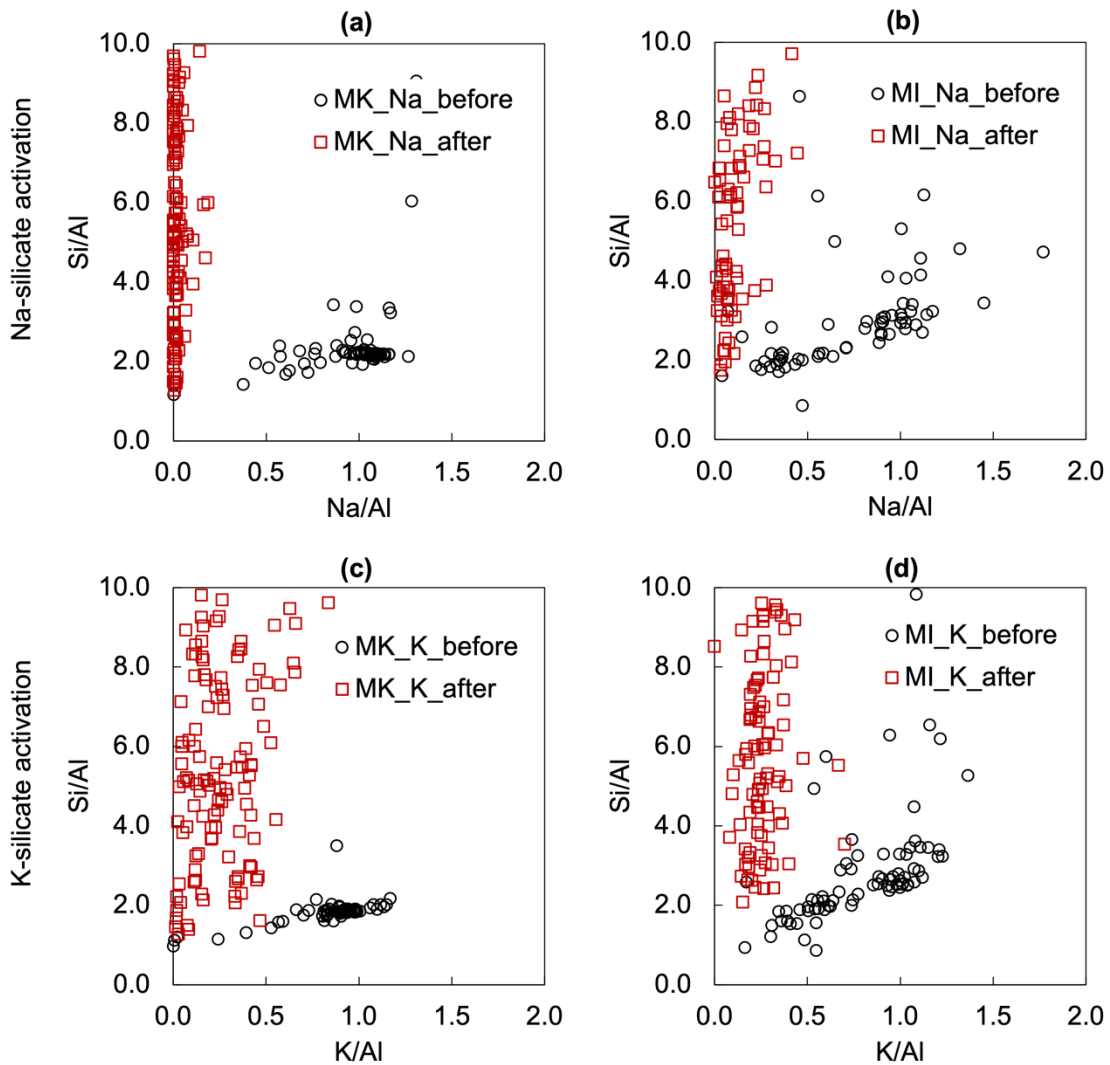
282 behavior of Al, concentrations increased with time for all the geopolymers (cf. Fig. 5b). In either case,
283 immersion solution of MI_Na geopolymer exhibited much lower Si and Al concentrations, especially for
284 the Si concentration, which was relatively stable during the test. In the case of the MI_K immersion
285 solution, Al and Si elements exhibited a rapid increase in concentration at the end of the test. Nonetheless,
286 Al concentrations were slightly higher in the MK_K immersion solution.

287 On the other hand, the trend of Ca leaching was similar for MK_Na, MK_K and MI_Na geopolymers
288 increasing linearly over time (cf. Fig. 5c). Among these three geopolymers, MI_Na presented a higher Ca
289 concentration in the immersion solution, which is explained by the greater initial concentration of Ca in
290 the meta-illite (cf. Table 1). On the contrary, the immersion solution of the MI_K geopolymer presented
291 very high Ca concentration at the beginning of the test and then leaching kinetics were less rapid.
292 Similarly, immersion solution of MK_Na, MK_K and MI_Na geopolymers exhibited a low release of Fe
293 into the solutions, with slightly higher concentrations of Fe for the MI_Na due to the composition of the
294 MI, which contains higher amounts of Fe. As for the Ca concentration in the MI_K immersion solution,
295 Fe concentrations were higher than those measured for the other geopolymers, and leaching kinetics were
296 very rapid (cf. Fig. 5d).

297 Finally, Fig. 5e and Fig. 5f present the degree of leaching of Na and K separately. Fig. 5e presents the
298 results obtained for geopolymers activated by Na-silicate, and Fig. 5f presents the results obtained for
299 geopolymers activated by K-silicate. Fig. 5e illustrates that Na release into the immersion solution
300 followed a similar trend in both immersion solutions, in which Na concentrations increased with time.
301 Nonetheless, the leaching coefficient (L_c) of Na was higher in the immersion solution of the MK_Na
302 geopolymer. Likewise, the release of K into the immersion solutions of MK_K and MI_K geopolymers
303 presented similar behavior (i.e., K concentration increased with the time of immersion). However, the
304 immersion solution of the MI_K geopolymer showed higher K concentrations than those measured for the
305 MK_K.

306 **3.4. SEM/EDS characterization**

307 Si/Al and R/Al (R=Na or K) molar ratios were determined by performing EDS pointing analyses in all the
308 geopolymers before attack (at 28 days of curing) and in the altered zones of geopolymers exposed to
309 sulfuric acid attack. Fig. 6 presents EDS pointing analyses in the form of mixing diagrams, where R/Al
310 molar ratios are plotted versus Si/Al molar ratios (x-axis and y-axis, respectively).



311

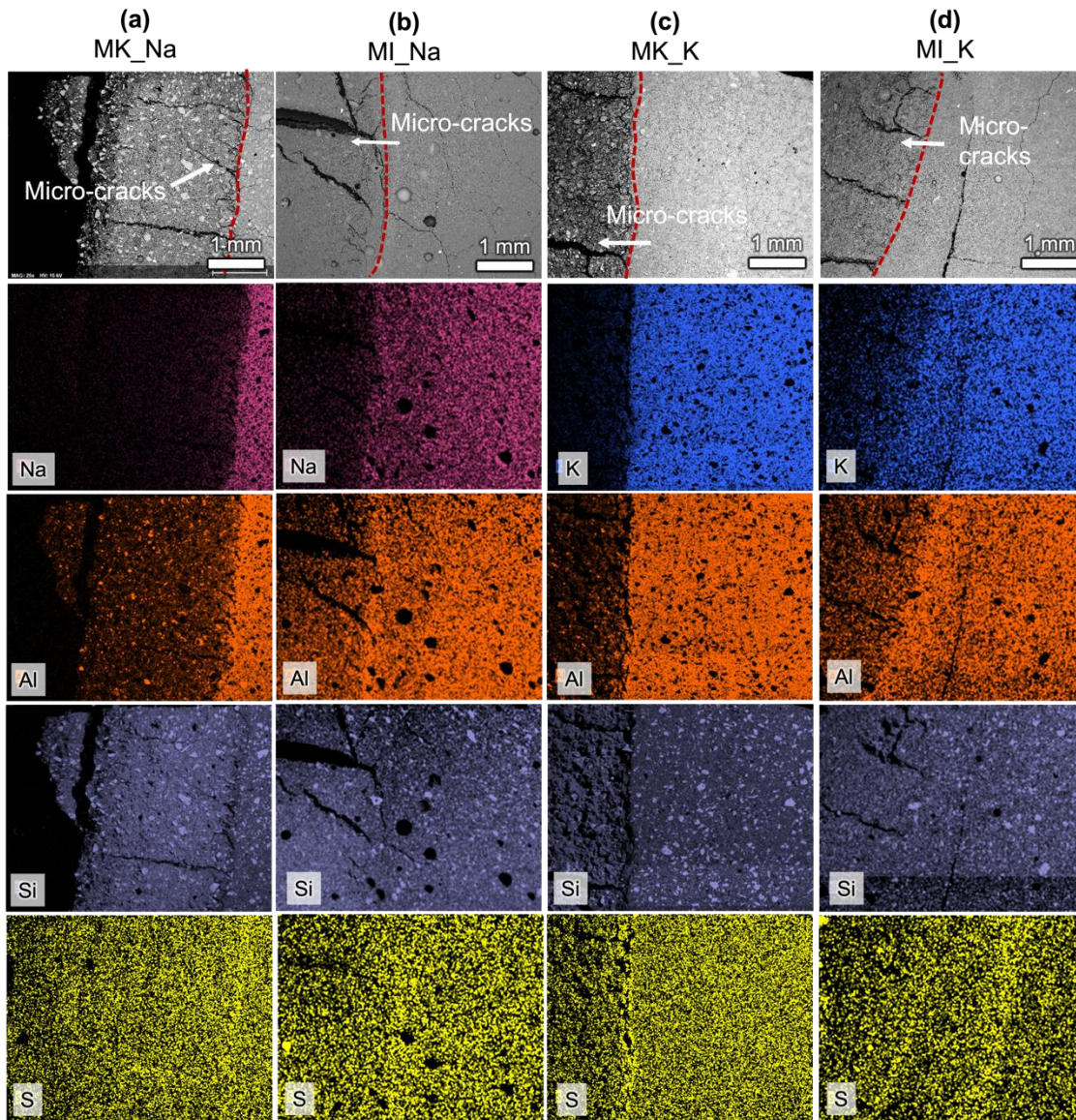
312 **Fig. 6.** EDS diagrams of Si/Al vs. R/Al molar ratios (R = Na or K) for all geopolymers before (black circles) and
313 after (red squares) sulfuric acid attack. After sulfuric acid attack, analyses were carried out on the altered zones (cf.
314 Fig. 4). (a) MK_Na, (b) MI_Na, (c) MK_K, and (d) MI_K.

315 Before attack, MI-based geopolymers exhibited the presence of two populations of points in the Si/Al vs.
316 R/Al charts, probably due to the presence of non-reactive illite content (about 19 wt. %), which may have
317 modified the R/Al (R = Na or K) molar ratios (cf. Fig. 6). This would partially explain why arithmetic
318 average values of Si/Al molar ratios obtained from MI-based geopolymers were slightly higher than those
319 determined in MK-based geopolymers ($2.5\% \pm 0.2\%$, $2.4\% \pm 0.2\%$, $2.2\% \pm 0.1\%$, $1.8\% \pm 0.1\%$ for MI_Na,
320 MI_K, MK_Na and MK_K, respectively) in addition to a higher amorphous content in the MI precursor
321 (cf. Table 2). Moreover, Si/Al molar ratios were higher in Na-silicate activated geopolymers (MK_Na and
322 MI_Na) than in K-silicate activated geopolymers (MK_K and MI_K). This is explained by the higher Si
323 concentration in the Na-silicate solution: 27.5% SiO₂ versus 24% SiO₂ in the K-silicate solution (cf.
324 section 2.1.2).

325 After attack, altered zones of geopolymers displayed higher dispersion of data than before attack.
326 Moreover, R/Al molar ratios decreased, while Si/Al molar ratios increased compared to the samples
327 before sulfuric acid attack, which suggests that Al and the alkali content (Na or K) decreased in the
328 altered zones of geopolymers exposed to sulfuric acid attack. These results are in line with the evolutions
329 of element concentrations determined in the immersion solutions (cf. Fig. 5) and further details will be
330 presented in the discussion section.

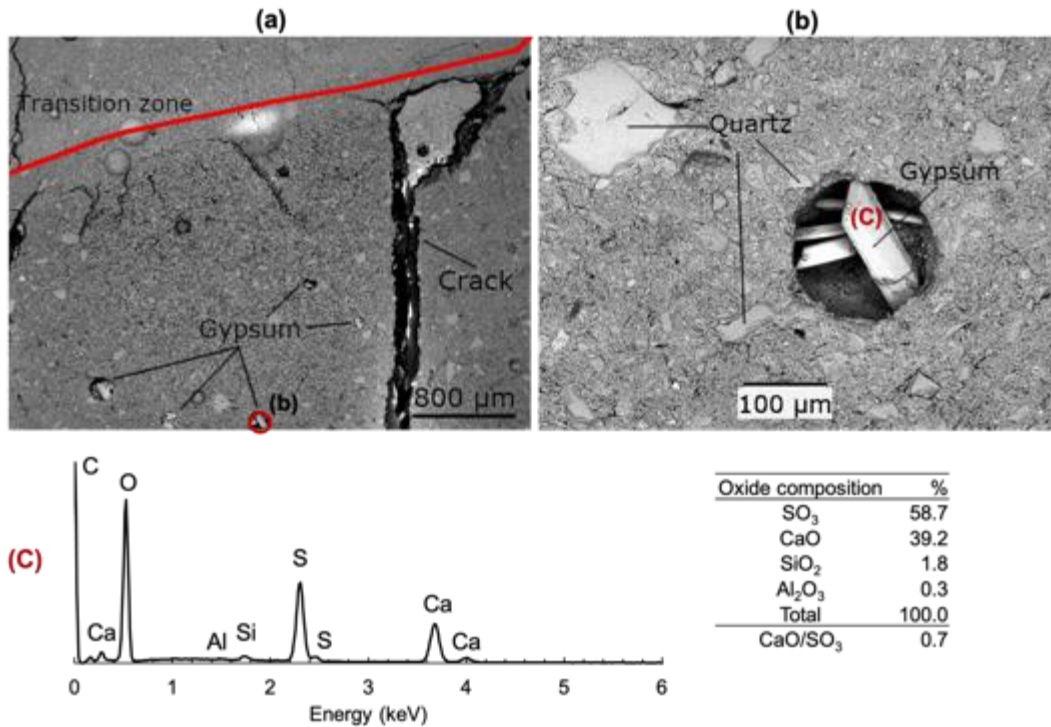
331 EDS mapping was performed on geopolymers after sulfuric acid attack to corroborate the leaching
332 behavior of elements in the altered zones. Fig. 7 displays EDS mapping for Al, Na, K, Si and S elements.
333 All geopolymers were characterized by the presence of two distinct zones referred to as altered and
334 unaltered zones. The transition between these two zones is marked by a red dotted line. Scans of Al, Na
335 and K elements showed that these elements dropped in concentration in the altered zones. Si and S scans
336 were difficult to interpret, possibly because Si concentrations were similar in altered and unaltered zones
337 (further information is presented in section 3.6, in which ²⁹Si NMR analyses are showed). Moreover, EDS
338 scans showed that S was not chemically bonded in the geopolymers except in the layer of the altered zone
339 of the MI_Na geopolymer, in which gypsum was identified. Fig. 8 presents images obtained from

340 SEM/EDS observations carried out on the altered layer of MI_Na geopolymers, showing the presence of
341 gypsum, which precipitated in the pore space, which may modify further ingress of sulfuric acid into the
342 matrix. Further discussion will be addressed in the discussion section 4.1.



343

344 **Fig. 7.** EDS mapping obtained from the scan of Na, K, Al, Si and S elements in polished surfaces of geopolymer
345 pastes after sulfuric acid attack. The red dashed line marks the border between altered (left) and unaltered zones
346 (right) (a) MK_Na, (b) MI_Na, (c) MK_K, and (d) MI_K.

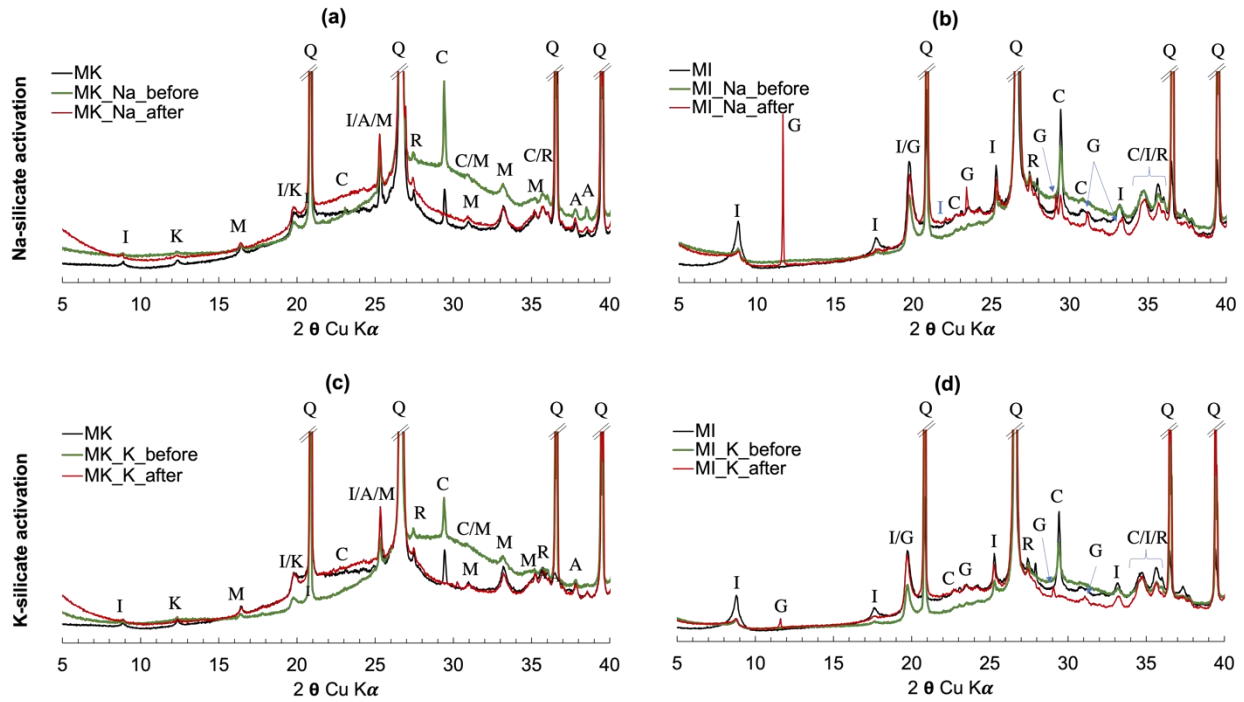


347

348 **Fig. 8.** SEM images of MI_Na geopolymer after sulfuric acid attack and EDS spectrum of gypsum. (a) Transition
 349 between altered (bottom) and unaltered zones, (b) zoom on one pore containing gypsum and located in image (a),
 350 and (c) EDS spectrum and oxide composition of gypsum found in a pore of the altered material.

351 3.5. XRD characterization

352 Fig. 9 presents XRD analyses performed on crushed samples taken from geopolymers before acid attack
 353 and from the altered layer of geopolymers exposed to sulfuric acid. All XRD patterns were plotted in the
 354 selected range of 2θ from 5° to 40° to zoom in on the main differences. XRD patterns from the precursors
 355 (MK and MI) are also plotted for comparison.



A: Anatase, C: Calcite, G: Gypsum, I: Illite, K: Kaolinite, M: Mullite, Q: Quartz, R: Rutile

356

357 **Fig. 9.** XRD patterns obtained from crushed geopolymers activated by Na-silicate (top) and by K-silicate (bottom),
 358 plotted in the selected range of 2θ from 5° to 40° to zoom in on the main differences. (a) MK_Na, (b) MI_Na, (c)
 359 MK_K, and (d) MI_K. **Black lines:** precursors (MK or MI). **Green lines:** geopolymers before attack. **Red lines:**
 360 altered layer of geopolymers after sulfuric acid attack.

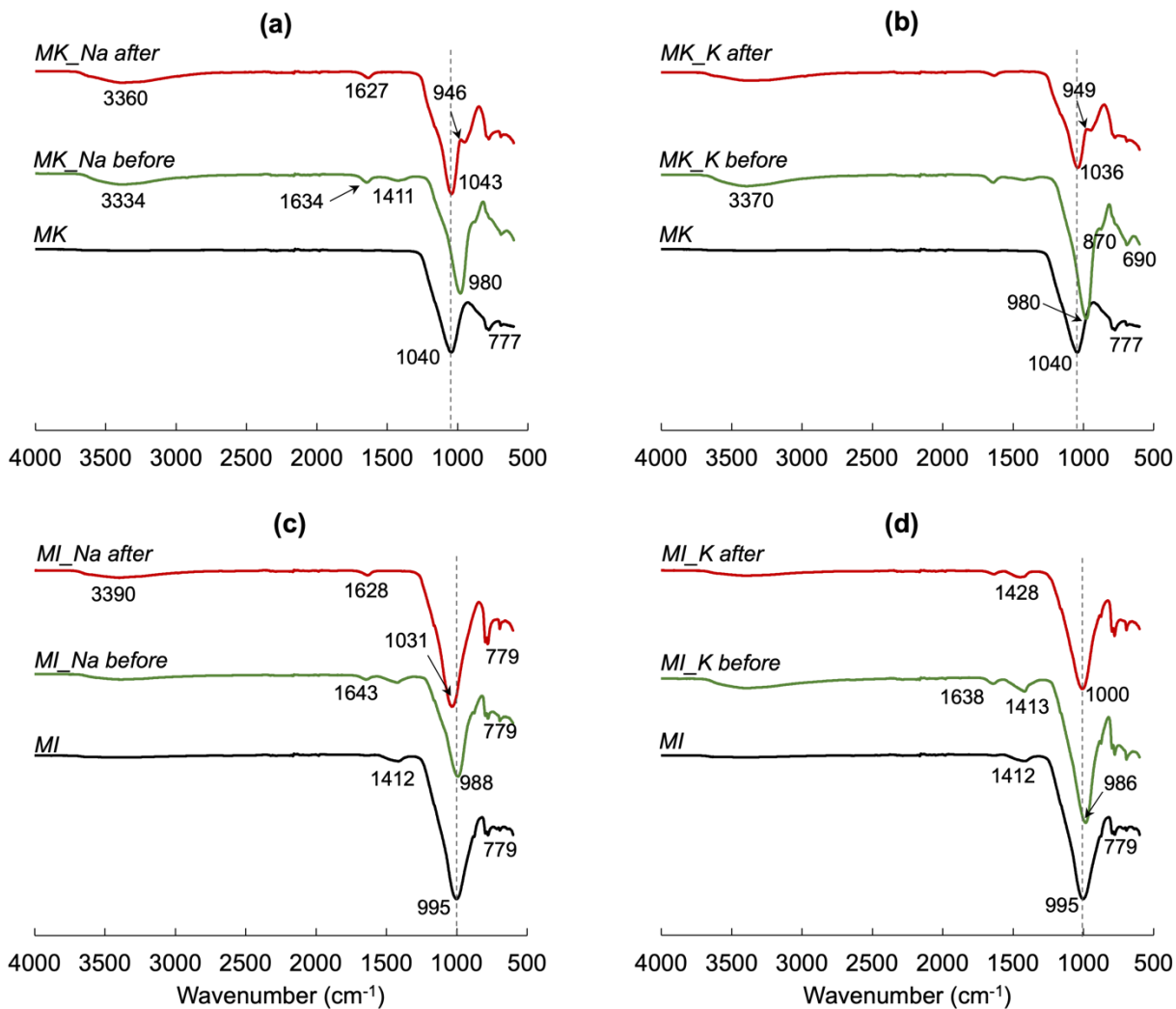
361 XRD patterns obtained from the precursors showed a semi-crystalline structure, in which several main
 362 common crystallized phases were identified as illite, kaolinite, calcite, rutile and quartz. MK precursor
 363 also displayed the presence of mullite and anatase. Patterns for both calcined clays presented a hump
 364 mainly centered at 2θ 26° - 27° , which was attributed to amorphous phases [22,43]. After the alkali
 365 activation process and before the sulfuric acid attack, these humps were broader and shifted toward higher
 366 degrees (2θ 29° - 30°) because of the activation, which was accompanied by an increase of the relative
 367 intensity of amorphous content. The relative intensity of these humps seemed higher in MK-based
 368 geopolymers than in MI-based geopolymers. Furthermore, peaks originally identified in the precursors
 369 remained in geopolymer patterns but with reduced relative intensity. This was mainly observed for illite

370 peaks at 2θ 8° - 10° and 2θ 17° - 18° in the XRD patterns of the MI_Na geopolymer. These minerals do not
371 normally participate in the geopolymerization process but present lower intensities due to a dilution effect
372 [22,28].

373 After sulfuric acid attack, XRD patterns from the altered zones presented the main crystallized phases
374 originally identified in calcined clays and in geopolymers before attack, except for calcite (main peak
375 situated at 2θ 29°), which disappeared from all geopolymer patterns after attack. Moreover, all patterns
376 exhibited a decrease in the relative intensity of the amorphous hump initially centered at 2θ 29° - 30° ,
377 which also shifted toward lower angles (2θ 22° - 26°). Altered zones of MI-based geopolymers displayed
378 the presence of gypsum (main peak at 2θ 11° - 12°). The relative intensity of the main peak of gypsum was
379 much lower in MI_K than in MI_Na.

380 **3.6. FT-IR and solid-state NMR characterization**

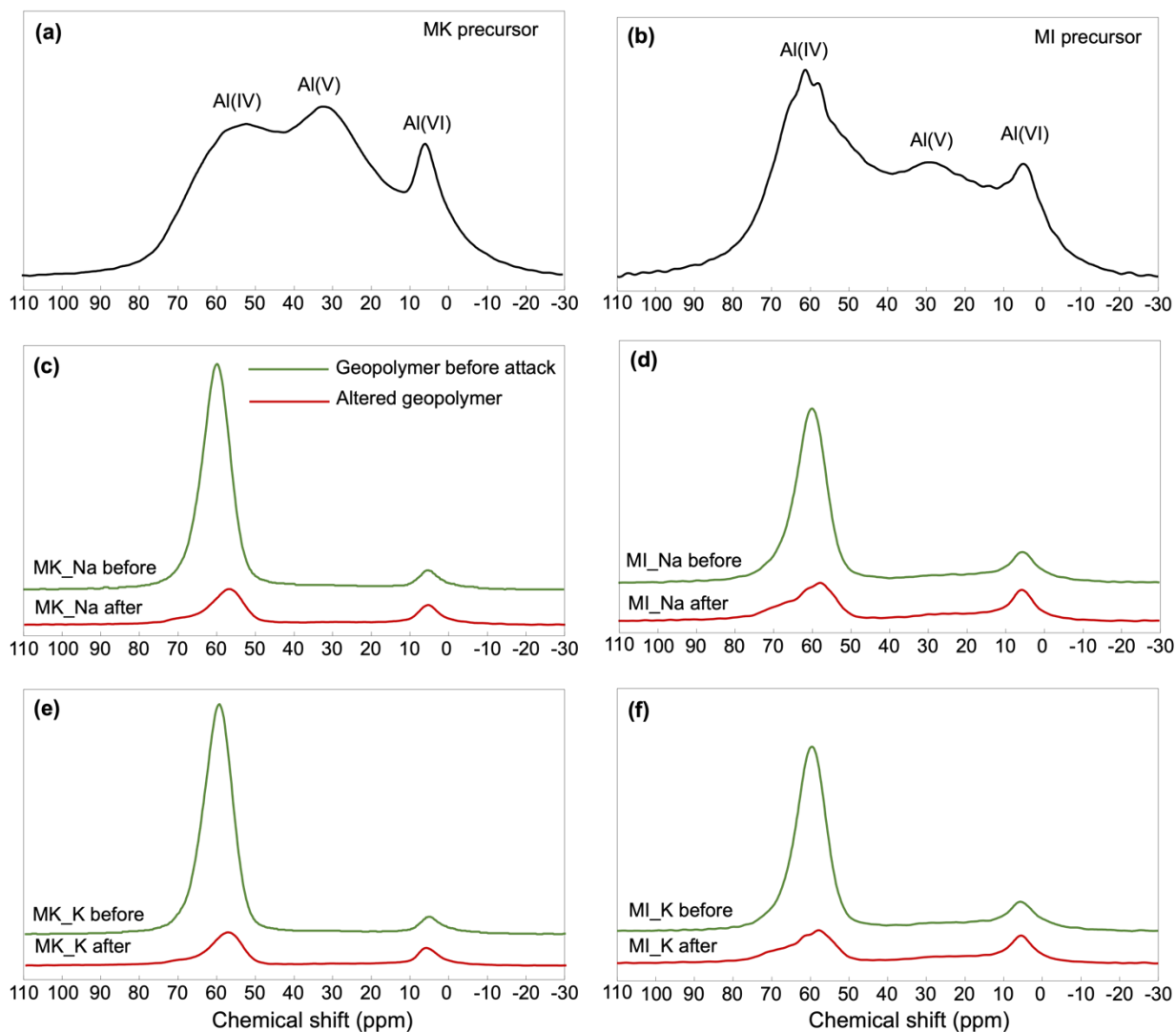
381 FT-IR spectra obtained from samples before sulfuric acid attack and from altered geopolymers were
382 plotted for wavenumbers ranging from 4000 cm^{-1} to 500 cm^{-1} and are presented in Fig. 10. Fig. 11
383 presents the ^{27}Al NMR spectra obtained from the precursors and from the geopolymers before and after
384 (altered layer) sulfuric acid attack. Finally, Fig. 12 shows the ^{29}Si NMR spectra of geopolymers before
385 and after (altered layer) acid attack for the MI_Na and MK_Na geopolymers.



386

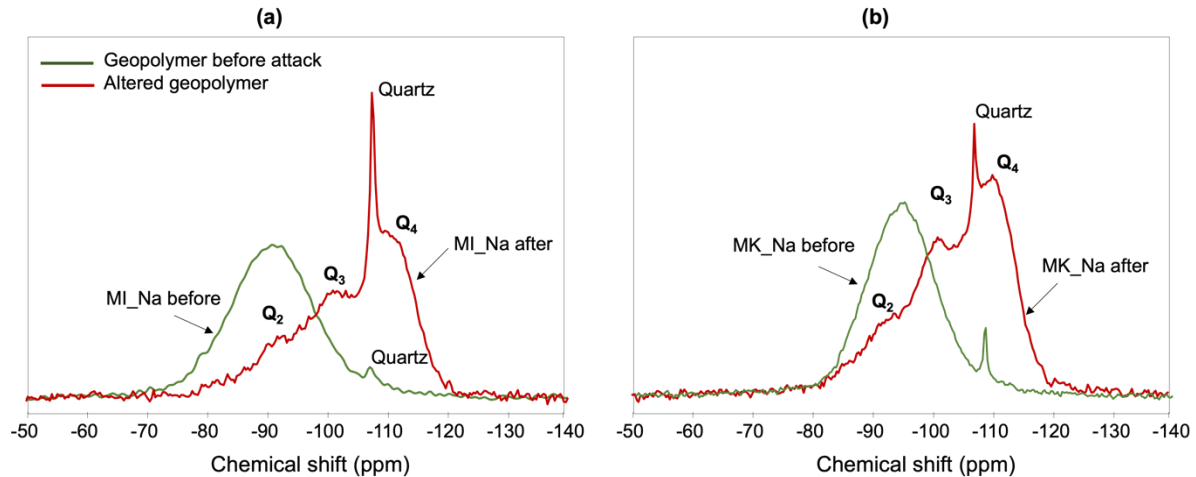
387 **Fig. 10.** FT-IR spectra obtained from crushed geopolymers before (green lines) and after (altered layer) sulfuric acid
 388 attack. (a) MK_Na, (b) MK_K, (c) MI_Na, and (d) MI_K. **Black lines:** precursors (MK or MI).

389



390

391 **Fig. 11.** ^{27}Al MAS NMR spectra (a) MK precursor, (b) MI precursor, (c) MK_Na, (d) MI_Na, (e) MK_K, and (f)
 392 MI_K. **Black lines:** precursors. **Green lines:** crushed geopolymers before sulfuric acid attack. **Red lines:** crushed
 393 altered layer from geopolymers after sulfuric acid attack. The relative intensities of Al(VI) were normalized before
 394 and after sulfuric acid attack for comparison.



395

396 **Fig. 12.** ^{29}Si MAS NMR spectra obtained from geopolymers activated by Na-silicate before and after sulfuric acid
 397 attack (a) MI_Na, and (b) MK_Na. After attack, spectra correspond to the altered layer identified in the
 398 geopolymers.

399 In FT-IR spectra, the main absorption bands and corresponding assignments identified in Fig. 10 were:
 400 $3600\text{-}3100\text{ cm}^{-1}$ (O-H stretching bands), O-H stretching bands of Si-OH and Al-OH groups appearing in
 401 $3700\text{-}3200\text{ cm}^{-1}$ (Si-OH and Al-OH stretching), $1500\text{-}1400\text{ cm}^{-1}$ (O-H deformation), $1130\text{-}900\text{ cm}^{-1}$
 402 (asymmetrical Si-O-T stretching vibrations, T = Al, Si), $900\text{-}850\text{ cm}^{-1}$ (asymmetric Si-OH and Al-OH
 403 stretching vibrations), and 795 cm^{-1} (symmetric stretching vibrations of Si-O-T, T = Al, Si) [16,44].
 404 Spectra obtained from the precursors showed that asymmetrical Si-O-T (T= Al, Si) stretching vibration
 405 bands were located at 1040 cm^{-1} and 995 cm^{-1} , respectively. After alkali activation and before sulfuric
 406 acid attack (green spectra), O-H stretching bands were identified at $3600\text{-}3100\text{ cm}^{-1}$ due to hydrogen
 407 bonding. Moreover, asymmetrical Si-O-T stretching bands (initially placed between 1040 cm^{-1} and
 408 995 cm^{-1}) shifted toward lower wavenumber values (about 980 cm^{-1}), which indicates that the degree of
 409 polymerization increased after alkali activation. According to the literature, substitution of Si by
 410 tetrahedral Al in the Si-O-Si network results in a shift of the Si-O-T asymmetric stretching band toward
 411 lower wavenumbers [45]. On the contrary, FT-IR spectra obtained from altered zones of geopolymers

412 exposed to sulfuric acid (red spectra) showed that asymmetrical Si-O-T stretching vibration bands shifted
413 toward higher wavenumber values and were narrower than those obtained before attack. FT-IR results are
414 consistent with XRD analyses, which may imply a modification of both the geopolymerization degree and
415 the structure of Si-O-T bonds after sulfuric acid exposure.

416 ²⁷Al NMR spectra obtained from the precursors showed the presence of Al in three different coordination
417 states: Al(IV), Al(V) and Al(VI) (cf. Fig. 11a and b). Moreover, the shape of the MI spectrum suggested
418 the coexistence of at least two different environments for Al(IV). After alkali activation, ²⁷Al NMR
419 spectra exhibited the presence of Al mainly in 4-fold coordination with small amounts of Al in 6-fold
420 coordination (around 6% for MK_Na and MK_K and 15% for MI_Na and MI_K). For MI-based
421 geopolymers, a small resonance of Al(V) can still be observed. These results are in line with the literature
422 showing that, after alkaline activation, Al in 5- and 6-fold coordination is mainly converted to 4-fold
423 coordination [19,25]. After sulfuric acid attack, ²⁷Al NMR of altered zones were more complex to
424 interpret. Spectra exhibited an increase in the proportion of Al(VI) and Al(V) and the existence of at least
425 two tetrahedral Al environments in both MK and MI geopolymers. Surface areas of all ²⁷Al NMR spectra
426 were calculated and compared to the spectra of geopolymers before attack to estimate the amount of Al
427 released from the altered zones. Table 6 summarizes the proportions of Al calculated to remain in the
428 altered layer of the geopolymers after sulfuric acid attack. Overall, calculations indicated that about 40-
429 60% of Al was released from the altered layers of the MI- and MK-based geopolymers.

430 Regarding the ²⁹Si NMR analyses, spectra obtained from MI or MK-based geopolymers activated by Na-
431 silicate showed the presence of Si in the form of silicate tetrahedra in three different environments (Q₂, Q₃
432 and Q₄). Before sulfuric acid, the main resonances were found at -90 ppm (Q₂) and at -110 ppm (Q₄), the
433 latter corresponding to quartz. In the altered zones, spectra shifted toward lower chemical shifts, and
434 tetrahedral silicate was mainly present in Q₃ and Q₄ environments. These results suggested that the
435 polymerization degree of Si increased after sulfuric acid attack. Further details will be presented in the
436 discussion section 4.3.

437 **Table 6** Calculated percentage (%) of total aluminum remaining in the altered layer of geopolymers after sulfuric
438 acid attack. Values were obtained with ^{27}Al NMR spectra taking the initial mass of each sample into account.

Geopolymer	MK_Na	MK_K	MI_Na	MI_K
Before attack	100	100	100	100
Altered layer	37	52	60	53

439

440 **4. Discussion**

441 **4.1. Behavior of geopolymers under sulfuric acid attack**

442 In this study, the resistance of four calcined clay-based geopolymers to sulfuric acid attack has been
443 investigated. To this end, geopolymers were exposed to aggressive conditions by the immersion of paste
444 samples in an H_2SO_4 solution at pH 1 for 30 days. The resistance of samples to sulfuric acid was assessed
445 by following the mass evolution and by direct observations. Results indicated that all geopolymers were
446 susceptible to sulfuric acid attack, but degradation degrees were slightly different. Overall, geopolymers
447 activated by Na-silicate were less likely to be damaged than those activated by K-silicate. In fact, MI_Na
448 geopolymer showed minor degradation compared to all the other geopolymers; its exposed surface
449 seemed to present the least damage (lower dissolution than the other geopolymers) even though some
450 vertical cracks were identified (cf. Fig. 4).

451 After 30 days of acid exposure, MI_Na geopolymer showed a gain in mass of about 1.4%. Meanwhile,
452 MK_Na, MK_K and MI_K geopolymers presented losses in mass of 1.5%, 2.0%, and 3.2%, respectively
453 (cf. Fig. 3). The initial gain in mass observed in all the materials (except for MI_K) may correspond to the
454 initial uptake of water at the beginning of the test. At the end of the test, the gain in mass in MI_Na
455 geopolymers could be partially explained by the precipitation of gypsum in the pore space of the altered
456 layer as determined by SEM/EDS (cf. Fig. 8) and verified by XRD analyses (cf. Fig. 9). The precipitation

457 of gypsum was explained by the reaction between Ca ions present in MI precursor ($\text{CaO} = 4.4 \text{ wt. } \%$) and
458 the sulfate ions present in the immersion solution. Altered zones of MI_K geopolymers also displayed the
459 presence of gypsum (cf. Fig. 9), but with a relative intensity much lower than that observed in altered
460 MI_Na. This may be due to the amount of material that was dissolved in the MI_K geopolymer during the
461 test. In contrast, gypsum did not precipitate in the altered zones of MK-based geopolymers, due to the
462 unavailability or very low concentration of Ca ($\text{CaO} = 0.7 \text{ wt. } \%$). Since the deterioration was very slight
463 in the surface of MI_Na geopolymers, it was assumed that the amount of gypsum was not deleterious to
464 the material. Instead, the formation of gypsum could help to fill pores and block further acid ingress into
465 the material. This phenomenon has also been reported in the literature for different low-Ca geopolymer
466 systems. Allahverdi and Škvára, 2005 [46] studied the resistance of a geopolymer (made by a
467 combination of fly ash and slag, activated by NaOH and a Na-silicate solution) to sulfuric acid (pH 1).
468 These authors explain that, during the acid attack, Ca ions exchanged with H^+ or H_3O^+ ions present in the
469 immersion solution and, during this process, Ca and sulfate reacted. This reaction led to the formation and
470 deposition of non-deleterious gypsum precipitates in the altered material.

471 Other investigations carried out on alternative binders under sulfuric acid attack have also shown that
472 such systems present mass loss over time. Bakharev, 2005 [16] studied the behavior of class F fly ash
473 geopolymer systems (activated by NaOH, KOH or Na-silicate) under 5% sulfuric acid solution. These
474 authors showed that all the geopolymers presented mass losses ranging from 2 to 12%. Similarly, Sata et
475 al., 2012b [47] studied the resistance of fly ash and lignite bottom ash geopolymers immersed in a
476 solution containing 3% sulfuric acid. They showed that geopolymer mortars presented mass losses
477 varying from 1.4 to 3.6%, which were much lower than those in OPC systems after 120 days of
478 immersion. In the present study, CEM I-based samples showed a gain in mass of 3.5% after 30 days of
479 immersion, probably due to the initial saturation of pores and the precipitation of gypsum. Since the
480 immersion solution was not renewed, the layer of altered materials remained in the material and, unlike
481 the situation in MK_Na, MK_K and MI_K geopolymers, no dissolution of the material was observed.

482 Longer examination of CEM I and MI_Na materials will need to be carried out to compare the
483 performance of materials when exposed to sulfuric acid.

484 **4.2. Methodology for the evaluation of sulfuric acid resistance: immersion procedure and**
485 **monitoring of elemental concentrations**

486 Sulfuric acid resistance was assessed by static immersion of geopolymer paste samples in sulfuric acid
487 solution at pH 1. This chemical test is not a bio-chemical investigation and therefore, it may present some
488 bias, such as the precipitation of products due to the equilibrium occurring with time between the material
489 and the non-renewed solutions. However, this static immersion test is a good way to select cementitious
490 binders to be used when acid attack is probable and in future bio-chemical applications (e.g., wastewater
491 networks, fermentation or methanogenesis environments).

492 The evolution of the leaching coefficients of the leached elements determined in the immersion solutions
493 (cf. Fig. 5) were well in line with the mass variation results (cf. Fig. 3). To compare the leaching degree
494 of geopolymers, total leaching coefficients (Lc) were calculated according to [41,42] and presented in
495 Table 7. Lc values are relative to the initial volume of samples, which was about 0.21 L per formulation,
496 which explains the low values of the coefficients determined per leached element and per formulation.
497 Moreover, the order of magnitude of the Lc values are in line with the low values of mass variations
498 obtained from the geopolymers during the sulfuric acid attack (cf. Fig. 3). As presented in Fig. 4,
499 geopolymer samples exhibited layers of dissolved material varying from 2 mm to 8 mm deep, which
500 represent a proportion of 3 to 10% of dissolved material compared to the initial volume of the geopolymer
501 pastes.

502 **Table 7** Total leaching coefficients (Lc) calculated for all the paste samples over time.

Time (d)	0.17	2	5	20	30	Total Lc
CEM I	0.03	0.06	0.08	0.19	0.25	0.61
MK_Na	0.08	0.85	1.54	2.60	2.83	7.90

MI_Na	0.02	0.33	0.53	0.99	1.32	3.19
MK_K	0.25	1.70	2.18	3.20	3.59	10.91
MI_K	0.04	1.47	2.02	2.77	4.03	10.34

503

504 Leaching coefficients (Lc) indicated that geopolymer pastes activated by K-silicate presented the highest
505 release of elements into the immersion solutions. Furthermore, Lc results corroborated that MI_Na
506 geopolymer was the material that presented the lowest deterioration among all geopolymers under
507 sulfuric acid attack, since the degree of leaching was about 3.5 times lower than the one calculated for
508 geopolymers activated by K-silicate (MK_K and MI_K) and about 2.5 times lower than that in the
509 MK_Na geopolymer. Nonetheless, total Lc in MI_Na was higher than the one calculated for the reference
510 material (CEM I), in which the total leaching coefficient was of about 0.61. This may be explained by a
511 different degradation mechanism that consisted in the leaching of Ca into the immersion solution due to
512 the decalcification of Ca-rich phases (e.g., portlandite and calcium silicate hydrates). In fact, the total
513 leaching coefficient of Ca calculated in the immersion solution of CEM I corresponded to about 72% of
514 its total leaching coefficient. Therefore, the swelling observed in CEM I samples (gain in mass of 3.5%)
515 can be attributed to the precipitation of sulfate-rich phases (e.g., gypsum) in the solid material, which has
516 already been demonstrated in the literature for Ca-rich materials [12,48]. The precipitation of expansive
517 phases due to the high amount of Ca in the cement may eventually lead to cracking and thus, the loss of
518 material and mechanical resistance.

519 On the other hand, the trend of Na⁺ or K⁺ release into the immersion solutions was similar for all the
520 geopolymers. This means that the kinetics of Na⁺ or K⁺ release into the immersion solution was rapid, and
521 concentrations increased with increasing exposure time (cf. Fig. 5). However, Na concentration was about
522 1.6 times higher in the MK_Na immersion solution than that measured in the MI_Na immersion solution
523 (cf. Fig. 5e). This suggests that the release of Na into the solution was more rapid in the MK_Na
524 geopolymer than in the MI_Na samples, which may dissolve the material in a much rapid rate, which

525 could be partially explained by the higher total porosity in the MK-based geopolymers, increasing the
526 diffusion rates. The EDS mapping results confirm that the relative concentration of Na and K dropped in
527 all the altered zones of geopolymers exposed to sulfuric acid (cf. Fig. 7). These results are in line with the
528 EDS pointing analyses, which showed that Si/Al and R/Al (R=Na or K) molar ratios were modified in the
529 altered zones of the geopolymers (cf. Fig. 6). Si/Al molar ratios increased in all the geopolymers,
530 suggesting that Al content decreased after attack. R/Al molar ratios dropped after sulfuric exposure, due
531 to a decrease in both Al and alkali content (Na or K).

532 **4.3. Degradation mechanisms of geopolymers under sulfuric acid attack**

533 According to the results previously discussed, the main hypothesis explaining the degradation
534 mechanisms of geopolymers is that the release of alkali cations (Na^+ or K^+) into the acid solution leads to
535 disequilibrium of the aluminosilicate geopolymer network (Si-O-Al). Al in 4-fold coordination needs
536 counter ions to respect electroneutrality, so the mechanism of degradation should be the breaking of the
537 Si-O-Al bonds and the depletion of Al in the material (cf. Table 6).

538 Mineralogical and structural analyses carried out on the altered layer of geopolymers indicated that
539 amorphous structures of all the samples were modified by the exposure to sulfuric acid. XRD patterns
540 displayed a decrease in the relative intensity of the hump characteristic of the amorphous network (cf. Fig.
541 9). Additionally, FT-IR analyses showed that the asymmetrical Si-O-T (T= Al, Si) stretching band shifted
542 toward higher wavenumbers, which is related to a modification of the Si-O-T bonds due to the release of
543 Al from the geopolymer network (cf. Fig. 10). ^{27}Al and ^{29}Si MAS NMR spectra confirmed the
544 modification of the structural environments of Al and Si after attack (cf. Fig. 11, Fig. 12 and Table 6).
545 Additional treatment of ^{27}Al MAS NMR spectra revealed that the signals attributed to Al(IV) decreased in
546 proportion by 72%, 62%, 57% and 62% in the altered geopolymers of MK_Na, MK_K, MI_Na and
547 MI_K, respectively compared to the proportions obtained from unaltered geopolymers. Moreover, ^{29}Si
548 MAS NMR spectra obtained from geopolymers activated by Na-silicate indicated an increase in the

549 polymerization of Si due to the transformation of tetrahedron environments from Q₂ to Q₄. This suggests
550 that the Si network was reorganized because of the absence of Al, leading to the formation of an
551 amorphous silica gel. Similar results have been observed in the literature for other systems exposed to
552 sulfuric acid attacks, in which a silica gel was likely to be formed in the altered layer of the materials as a
553 result of the decomposition of Si-rich phases [48–50]. Moreover, FT-IR spectra of geopolymers after
554 attack presented a slight modification in the O-H stretching bands at 3700-3100 cm⁻¹, which indicated an
555 increase of Si-OH and Al-OH groups due to the sulfuric acid attack. Bakharev, 2005 [16] explained that
556 exposure of class F fly ash geopolymers to strong acidic solutions increased the number of Si-OH and Al-
557 OH groups following the breakage of Si-O-Al bonds. This phenomenon could be confirmed by
558 performing ¹H MAS NMR analyses coupled with ²⁷Al MAS NMR investigations. However, the
559 geopolymers studied in this investigation contained amounts of Fe that led to paramagnetic perturbations
560 and no such results were exploitable.

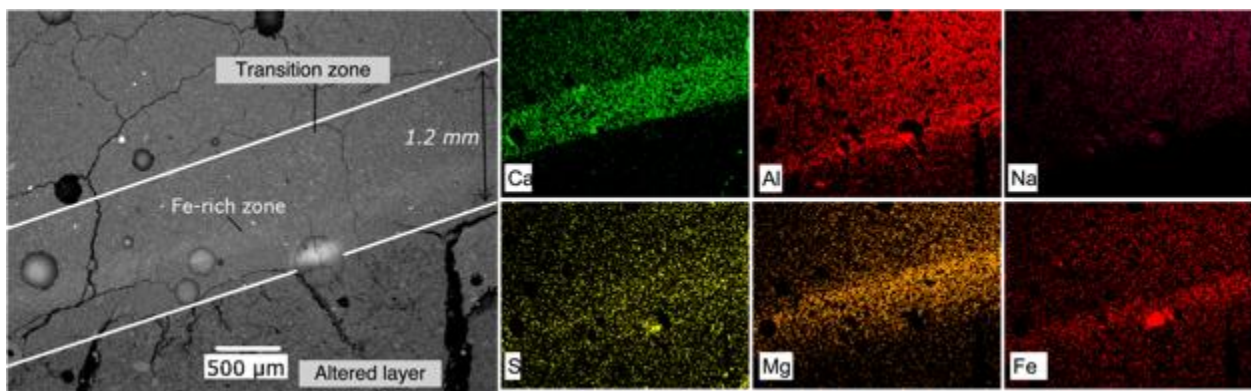
561 In addition, geopolymers activated by K-silicate exhibited highly altered surfaces (cf. Fig. 4) and high
562 leaching coefficients of leached elements in the immersion solutions (cf. Fig. 5). The porosity of these
563 materials may partially explain these results. In fact, the total porosities accessible to mercury of
564 geopolymers activated by K-silicate were slightly higher than those determined in geopolymers activated
565 by Na-silicate (cf. Table 4). According to the literature, geopolymers activated by K-activating solutions
566 seem to present greater degradation than those activated by Na-activating solutions [5,29]. Grengg et al.,
567 2021 [30] studied MK-based geopolymers activated by K-silicate (SiO₂/K₂O ratio of 0.95) under sulfuric
568 acid attack at pH 2. These authors showed that samples presented a complete dissolution of the
569 geopolymer structure and the formation of a silica gel in the altered materials. Vogt et al., 2020 [29] also
570 studied an MK-based geopolymer activated by K-silicate under sulfuric acid at pH 1. They suggested that
571 the geopolymer degradation was first due to the leaching of K⁺ ions into the immersion solution, followed
572 by the dealumination and depolymerization of the geopolymer.

573 **4.4. Performance of MI-based geopolymers under sulfuric acid attack**

574 To the best of the authors' knowledge, no studies of MI-based geopolymers under sulfuric acid attack are
575 available in the literature. This investigation showed that MI-based geopolymers activated by Na-silicate
576 resisted sulfuric acid attack well. This was attributed to a combination of properties, such as the mineral
577 structure of illite, the chemical composition of the MI and the transfer properties of the geopolymer
578 pastes. The mineral structure of the illite (2:1 clay mineral) consists of repetitive tetrahedral and
579 octahedral cation sheets [22,33] which should reduce the availability of Al cations and thus decrease the
580 dissolution of Al when it is exposed to sulfuric acid attack. Regarding the total porosity accessible to
581 mercury, MI_Na pastes presented the lowest values of all the geopolymers (cf. Table 4), which may have
582 contributed to a less rapid diffusion of the aggressive ions into the solid material.

583 Additionally, EDS mapping performed on MI_Na geopolymers resulted in the identification of a layer
584 about 1 mm thick occurring in the transition zone between altered and unaltered zones. This phenomenon
585 was only identified in MI_Na geopolymer. Fig. 13 presents SEM/EDS analyses obtained from the MI_Na
586 exhibiting this transition zone after attack. The zone was composed of different layers of elements
587 (mainly Mg, Ca, and Fe). XRD analyses performed on the surface of this layer did not reveal the
588 formation of any crystalline Mg or Fe-rich phase but an increase in calcite. These observations may
589 suggest the formation of a protective gel layer preventing further degradation of the material. Gevaudan et
590 al., 2021 [31] studied the influence of Fe content on the resistance of MK geopolymers to sulfuric acid
591 (pH 2). They suggested that Fe-rich phases such as hematite could improve the acid resistance of
592 geopolymers activated by Na activating solutions, especially at high Na/Al ratios (> 1.39). The MI
593 precursor used in this study contained 7 wt. % Fe_2O_3 , which is twice that of the MK precursor (cf. Table
594 1). Surprisingly, MI_K geopolymer did not exhibit behavior similar to that of MI_Na. For MI_K
595 geopolymer, the release of Fe into the immersion solution was 76% higher than that from MI_Na. This
596 could be explained by the higher total porosity of MI_K (30.8%) compared to the porosity of MI_Na
597 (26.5%), which may have been influenced by the alkaline solution used for activation. Bakharev, 2005
598 [16] has shown that class F fly ash geopolymers activated by KOH and exposed to 5% sulfuric acid

599 solution presented 12.43% of mass loss, against 2.56% obtained from the same material activated by Na-
600 silicate. The authors mention that the activation of the fly ashes by KOH increased the average pore
601 diameter and reduced the material's resistance to sulfuric acid attack. Further analyses should be carried
602 out in calcined clay geopolymers by using techniques with much lower detection limits (e.g., MET) to
603 better understand degradation mechanisms and to discard similar local behaviors. Moreover, MK-based
604 geopolymers activated by Na-silicate and containing more than 7 wt. % Fe_2O_3 could be tested in order to
605 corroborate the influence of Fe present in the precursor on the sulfuric resistance of the geopolymers.



606
607 **Fig. 13.** BSE image and EDS mapping obtained from the scan of Ca, Al, Na, S, Mg and Fe elements in MI_Na
608 geopolymer paste after sulfuric acid attack. White solid lines demarcate the transition between altered and unaltered
609 zones.

610 Compared to other cementitious materials reported in the literature, calcined clay geopolymers appear to
611 show promising performance under sulfuric acid attack, since their mass variations have been relatively
612 low. Experimental tests should be carried out on calcined-clay geopolymers under similar and less
613 aggressive conditions and the results compared to those of other materials such as calcium aluminate
614 cements (CAC), which are well known for having higher resistance to a biogenic acid attack than OPC, in
615 both *in-situ* and laboratory conditions [51–53]. Finally, the study of geopolymers in the form of paste
616 samples allows to carry out mineralogical and microscopical characterizations of these materials and to
617 better understand their behavior under sulfuric acid attack. The investigation of geopolymers in the form

618 of pastes also gives insights into the degradation of these materials for their use as protective coating of
619 structures exposed to aggressive environments. However, the behavior of geopolymer pastes under
620 sulfuric acid attack should be compared to those of mortars and concrete to verify the kinetics of
621 degradation and to assess the influence of other parameters on the resistance to sulfuric acid attack.

622 **5. Conclusions**

623 Findings in this paper allowed the behavior of different calcined clay based geopolymers under sulfuric
624 acid (H_2SO_4) attack to be compared by using highly aggressive conditions. Moreover, this study gave
625 insights into the degradation mechanisms of meta-illite based geopolymers exposed to sulfuric acid,
626 which had not been addressed in the literature until now. In this study, metakaolin (MK) and meta-illite
627 (MI) precursors were activated by two different alkaline solutions (Na-silicate and K-silicate). Thus, four
628 different geopolymer pastes were studied: one MK-based geopolymer activated by Na-silicate (MK_Na),
629 one MK-based geopolymer activated by K-silicate (MK_K), one MI-based geopolymer activated by Na-
630 silicate (MI_Na), and one MI-based geopolymer activated by K-silicate (MI_K). After 28 days of curing,
631 samples were submerged in an H_2SO_4 solution at pH 1 for 30 days.

632 The main conclusions drawn from this study were:

- 633 1. All geopolymers were susceptible to degradation after sulfuric acid attack at pH 1. Overall, paste
634 samples presented a layer of altered material after exposure to sulfuric acid.
- 635 2. MK_Na, MK_K and MI_K geopolymers lost mass during the test, unlike MI_Na geopolymer, in
636 which the exposed surface seemed to be the least altered surface of all the geopolymers. Element
637 concentrations determined in the immersion solution of MI_Na were very low compared to those
638 in the solutions of the other geopolymers.
- 639 3. Gain in mass in the MI_Na geopolymer was explained by the saturation of pores due to the
640 immersion process and to the precipitation of non-deleterious gypsum in the altered layer.

- 641 4. Geopolymers activated by K-silicate solution (MK_K and MI_K) exhibited highly dissolved
642 surfaces leading to the mass loss of the material.
- 643 5. The general degradation mechanism in all geopolymers consisted of the release of alkalis (Na⁺
644 and K⁺) into the solution by the exchange with H⁺ and H₃O⁺ ions. This was followed by the
645 disequilibrium of the geopolymer phase (Si-O-Al) and, therefore, the release of Al into the
646 solution.
- 647 6. MI_Na geopolymers seemed to present a better resistance to sulfuric acid attack, which was
648 attributed to a combination of various factors: the mineral structure of illite, the transfer
649 properties, the chemical composition of the MI as well as the small precipitation of gypsum in the
650 altered zone, probably blocking further ingress of solution into the paste. Additionally, the
651 formation of an Fe-rich layer deposited in the transition zone between altered and unaltered
652 geopolymer may constitute a protective barrier inhibiting further degradation.
- 653 7. Despite degradation of geopolymers due to the highly aggressive conditions, the low mass
654 variations determined during the tests hold promise for improving the durability of materials
655 under sulfuric acid attack. The performance of these materials should be tested under less
656 aggressive conditions, for longer exposure times and on mortars and concrete samples to compare
657 degradation mechanisms.

658 **CRedit author statement**

659 **Laura Diaz Caselles:** Investigation, Formal analysis, Writing – original draft, Project administration.

660 **Bastien Balsamo:** Investigation, Methodology, Writing – Review & editing, Project administration.

661 **Virginie Benavent:** Conceptualization, Validation, Writing – review & editing. **Vincent Trincal:**

662 Conceptualization, Writing – review & editing. **Hugo Lahalle:** Conceptualization, Validation. **Cedric**

663 **Patapy:** Conceptualization, Writing – review & editing. **Valérie Montouillout:** Formal analysis, Writing

664 – review & editing. **Martin Cyr:** Supervision, Writing – review & editing, Funding acquisition, Project
665 administration.

666 **Declaration of competing interest**

667 The authors declare no conflict of interest.

668 **Acknowledgements**

669 This work was supported by the L2A project funded by EDF, VINCI CONSTRUCTION, VICAT,
670 ARGECO DEVELOPMENT, ECOCEM and the MBCC Group. Financial support from the IR-RMH-
671 THC FR3050 CNRS for conducting the research is gratefully acknowledged.

672 **References**

673 [1] A.G. Boon, Septicity in sewers: Causes, consequences and containment, *Water Science and*
674 *Technology*. 31 (1995). [https://doi.org/10.1016/0273-1223\(95\)00341-J](https://doi.org/10.1016/0273-1223(95)00341-J).

675 [2] A. Aboulela, M. Peyre Lavigne, A. Buvignier, M. Fourré, M. Schiettekatte, T. Pons, C. Patapy, O.
676 Robin, M. Bounouba, E. Paul, A. Bertron, Laboratory Test to Evaluate the Resistance of
677 Cementitious Materials to Biodeterioration in Sewer Network Conditions, *Materials*. 14 (2021)
678 686. <https://doi.org/10.3390/ma14030686>.

679 [3] N.I. Fattuhi, B.P. Hughes, The performance of cement paste and concrete subjected to sulphuric
680 acid attack, *Cement and Concrete Research*. 18 (1988) 545–553. [https://doi.org/10.1016/0008-](https://doi.org/10.1016/0008-8846(88)90047-6)
681 [8846\(88\)90047-6](https://doi.org/10.1016/0008-8846(88)90047-6).

682 [4] L. Gu, T. Bennett, P. Visintin, Sulphuric acid exposure of conventional concrete and alkali-
683 activated concrete: Assessment of test methodologies, *Construction and Building Materials*. 197
684 (2019) 681–692. <https://doi.org/10.1016/j.conbuildmat.2018.11.166>.

- 685 [5] C. Grengg, F. Mittermayr, N. Ukrainczyk, G. Koraimann, S. Kienesberger, M. Dietzel, Advances
686 in concrete materials for sewer systems affected by microbial induced concrete corrosion: A
687 review, *Water Research*. 134 (2018) 341–352. <https://doi.org/10.1016/j.watres.2018.01.043>.
- 688 [6] J. Monteny, E. Vincke, A. Beeldens, N. De Belie, L. Taerwe, D. Van Gemert, W. Verstraete,
689 Chemical, microbiological, and in situ test methods for biogenic sulfuric acid corrosion of
690 concrete, *Cement and Concrete Research*. 30 (2000) 623–634. [https://doi.org/10.1016/S0008-
691 8846\(00\)00219-2](https://doi.org/10.1016/S0008-8846(00)00219-2).
- 692 [7] M. Alexander, A. Bertron, N. De Belie, eds., *Performance of Cement-Based Materials in*
693 *Aggressive Aqueous Environments*, Springer Netherlands, Dordrecht, 2013.
694 <https://doi.org/10.1007/978-94-007-5413-3>.
- 695 [8] T.A. Aiken, W. Sha, J. Kwasny, M.N. Soutsos, Resistance of geopolymer and Portland cement
696 based systems to silage effluent attack, *Cement and Concrete Research*. 92 (2017) 56–65.
697 <https://doi.org/10.1016/j.cemconres.2016.11.015>.
- 698 [9] A.P. Joseph, J. Keller, H. Bustamante, P.L. Bond, Surface neutralization and H₂S oxidation at
699 early stages of sewer corrosion: Influence of temperature, relative humidity and H₂S
700 concentration, *Water Research*. 46 (2012) 4235–4245.
701 <https://doi.org/10.1016/j.watres.2012.05.011>.
- 702 [10] D.. Roberts, D. Nica, G. Zuo, J.. Davis, Quantifying microbially induced deterioration of concrete:
703 initial studies, *International Biodeterioration & Biodegradation*. 49 (2002) 227–234.
704 [https://doi.org/10.1016/S0964-8305\(02\)00049-5](https://doi.org/10.1016/S0964-8305(02)00049-5).
- 705 [11] T. Mori, T. Nonaka, K. Tazaki, M. Koga, Y. Hikosaka, S. Noda, Interactions of nutrients, moisture
706 and pH on microbial corrosion of concrete sewer pipes, *Water Research*. 26 (1992) 29–37.
707 [https://doi.org/10.1016/0043-1354\(92\)90107-F](https://doi.org/10.1016/0043-1354(92)90107-F).

- 708 [12] B. Huber, H. Hilbig, J.E. Drewes, E. Müller, Evaluation of concrete corrosion after short- and
709 long-term exposure to chemically and microbially generated sulfuric acid, *Cement and Concrete*
710 *Research*. 94 (2017) 36–48. <https://doi.org/10.1016/j.cemconres.2017.01.005>.
- 711 [13] V. Sata, A. Sathonsaowaphak, P. Chindapasirt, Resistance of lignite bottom ash geopolymer
712 mortar to sulfate and sulfuric acid attack, *Cement and Concrete Composites*. 34 (2012) 700–708.
713 <https://doi.org/10.1016/j.cemconcomp.2012.01.010>.
- 714 [14] A. Mehta, R. Siddique, Sulfuric acid resistance of fly ash based geopolymer concrete,
715 *Construction and Building Materials*. 146 (2017) 136–143.
716 <https://doi.org/10.1016/j.conbuildmat.2017.04.077>.
- 717 [15] M.A.M. Ariffin, M.A.R. Bhutta, M.W. Hussin, M. Mohd Tahir, N. Aziah, Sulfuric acid resistance
718 of blended ash geopolymer concrete, *Construction and Building Materials*. 43 (2013) 80–86.
719 <https://doi.org/10.1016/j.conbuildmat.2013.01.018>.
- 720 [16] T. Bakharev, Resistance of geopolymer materials to acid attack, *Cement and Concrete Research*.
721 35 (2005) 658–670. <https://doi.org/10.1016/j.cemconres.2004.06.005>.
- 722 [17] P.H. Simatupang, Characteristics of alkali activated material (geopolymer) in sulfuric acid
723 solution, in: 2017: p. 020028. <https://doi.org/10.1063/1.5003511>.
- 724 [18] R. Alzebaree, A. Çevik, B. Nematollahi, J. Sanjayan, A. Mohammedameen, M.E. Gülşan,
725 Mechanical properties and durability of unconfined and confined geopolymer concrete with fiber
726 reinforced polymers exposed to sulfuric acid, *Construction and Building Materials*. 215 (2019)
727 1015–1032. <https://doi.org/10.1016/j.conbuildmat.2019.04.165>.
- 728 [19] M.C.G. Juenger, F. Winnefeld, J.L. Provis, J.H. Ideker, Advances in alternative cementitious
729 binders, *Cement and Concrete Research*. 41 (2011) 1232–1243.

- 730 <https://doi.org/10.1016/j.cemconres.2010.11.012>.
- 731 [20] P. Duxson, J.L. Provis, Designing precursors for geopolymer cements, *Journal of the American*
732 *Ceramic Society*. 91 (2008) 3864–3869. <https://doi.org/10.1111/j.1551-2916.2008.02787.x>.
- 733 [21] J.L. Provis, Activating solution chemistry for geopolymers, *Geopolymers: Structures, Processing,*
734 *Properties and Industrial Applications*. (2009) 50–71.
735 <https://doi.org/10.1533/9781845696382.1.50>.
- 736 [22] R. Jaskulski, D. Józwiak-Niedźwiedzka, Y. Yakymchko, Calcined Clay as Supplementary
737 *Cementitious Material*, *Materials*. 13 (2020) 4734. <https://doi.org/10.3390/ma13214734>.
- 738 [23] S. Sperinck, P. Raiteri, N. Marks, K. Wright, Dehydroxylation of kaolinite to metakaolin—a
739 *molecular dynamics study*, *J. Mater. Chem*. 21 (2011) 2118–2125.
740 <https://doi.org/10.1039/C0JM01748E>.
- 741 [24] A.Z. Khalifa, Ö. Cizer, Y. Pontikes, A. Heath, P. Patureau, S.A. Bernal, A.T.M. Marsh, *Advances*
742 *in alkali-activation of clay minerals*, *Cement and Concrete Research*. 132 (2020) 106050.
743 <https://doi.org/10.1016/j.cemconres.2020.106050>.
- 744 [25] P. Duxson, A. Fernández-Jiménez, J.L. Provis, G.C. Lukey, A. Palomo, J.S.J. Van Deventer,
745 *Geopolymer technology: The current state of the art*, *Journal of Materials Science*. 42 (2007)
746 2917–2933. <https://doi.org/10.1007/s10853-006-0637-z>.
- 747 [26] Q.H. Nguyen, M. Hanafi, J. Merkl, J. d’Espinoze de Lacaillerie, *Evolution of the microstructure of*
748 *unconsolidated geopolymers by thermoporometry*, *Journal of the American Ceramic Society*. 104
749 (2021) 1581–1591. <https://doi.org/10.1111/jace.17543>.
- 750 [27] X.X. Gao, P. Michaud, E. Joussein, S. Rossignol, *Behavior of metakaolin-based potassium*
751 *geopolymers in acidic solutions*, *Journal of Non-Crystalline Solids*. 380 (2013) 95–102.

- 752 <https://doi.org/10.1016/j.jnoncrysol.2013.09.002>.
- 753 [28] K. Bouguermouh, N. Bouzidi, L. Mahtout, L. Pérez-Villarejo, M.L. Martínez-Cartas, Effect of
754 acid attack on microstructure and composition of metakaolin-based geopolymers: The role of
755 alkaline activator, *Journal of Non-Crystalline Solids*. 463 (2017) 128–137.
756 <https://doi.org/10.1016/j.jnoncrysol.2017.03.011>.
- 757 [29] O. Vogt, C. Ballschmiede, N. Ukrainczyk, E. Koenders, Evaluation of Sulfuric Acid-Induced
758 Degradation of Potassium Silicate Activated Metakaolin Geopolymers by Semi-Quantitative
759 SEM-EDX Analysis, *Materials*. 13 (2020) 4522. <https://doi.org/10.3390/ma13204522>.
- 760 [30] C. Grengg, G.J.G. Gluth, F. Mittermayr, N. Ukrainczyk, M. Bertmer, A. Guilherme Buzanich, M.
761 Radtke, A. Leis, M. Dietzel, Deterioration mechanism of alkali-activated materials in sulfuric acid
762 and the influence of Cu: A micro-to-nano structural, elemental and stable isotopic multi-proxy
763 study, *Cement and Concrete Research*. 142 (2021) 106373.
764 <https://doi.org/10.1016/j.cemconres.2021.106373>.
- 765 [31] J.P. Gevaudan, B. Santa-Ana, W. V. Srubar, Iron mineral admixtures improve the sulfuric acid
766 resistance of low-calcium alkali-activated cements, *Cement and Concrete Composites*. 116 (2021)
767 103867. <https://doi.org/10.1016/j.cemconcomp.2020.103867>.
- 768 [32] R. Lemma, E.F. Irassar, V. Rahhal, Calcined Illitic Clays as Portland Cement Replacements, in:
769 2015: pp. 269–276. https://doi.org/10.1007/978-94-017-9939-3_33.
- 770 [33] A. Meunier, *Clays*, 1st ed., Springer-Verlag, Berlin/Heidelberg, 2005.
771 <https://doi.org/10.1007/b138672>.
- 772 [34] V. Trincal, D. Charpentier, M.D. Buatier, B. Grobety, B. Lacroix, P. Labaume, J.-P. Sizun,
773 Quantification of mass transfers and mineralogical transformations in a thrust fault (Monte

- 774 Perdido thrust unit, southern Pyrenees, Spain), *Marine and Petroleum Geology*. 55 (2014) 160–
775 175. <https://doi.org/10.1016/j.marpetgeo.2013.12.016>.
- 776 [35] H. Lahalle, V. Benavent, V. Trincal, T. Wattez, R. Bucher, M. Cyr, Robustness to water and
777 temperature, and activation energies of metakaolin-based geopolymer and alkali-activated slag
778 binders, *Construction and Building Materials*. 300 (2021) 124066.
779 <https://doi.org/10.1016/j.conbuildmat.2021.124066>.
- 780 [36] A. Hasnaoui, Optimisation d'un géopolymère à base de laitier et de metakaolin pour la réalisation
781 d'un béton de structure, 2019.
- 782 [37] D. Massiot, F. Fayon, M. Capron, I. King, S. Le Calvé, B. Alonso, J.-O. Durand, B. Bujoli, Z.
783 Gan, G. Hoatson, Modelling one- and two-dimensional solid-state NMR spectra, *Magnetic
784 Resonance in Chemistry*. 40 (2002) 70–76. <https://doi.org/10.1002/mrc.984>.
- 785 [38] V. Trincal, V. Benavent, H. Lahalle, B. Balsamo, G. Samson, C. Patapy, Y. Jainin, M. Cyr, Effect
786 of drying temperature on the properties of alkali-activated binders - Recommendations for sample
787 preconditioning, *Cement and Concrete Research*. 151 (2022) 106617.
788 <https://doi.org/10.1016/j.cemconres.2021.106617>.
- 789 [39] V. Benavent, F. Frizon, A. Poulesquen, Effect of composition and aging on the porous structure of
790 metakaolin-based geopolymers, *Journal of Applied Crystallography*. 49 (2016) 2116–2128.
791 <https://doi.org/10.1107/S1600576716014618>.
- 792 [40] P. Steins, A. Poulesquen, F. Frizon, O. Diat, J. Jestin, J. Causse, D. Lambertin, S. Rossignol,
793 Effect of aging and alkali activator on the porous structure of a geopolymer, *Journal of Applied
794 Crystallography*. 47 (2014) 316–324. <https://doi.org/10.1107/S160057671303197X>.
- 795 [41] C. Lors, E.D. Hondjuila Miokono, D. Damidot, Interactions between *Halothiobacillus*

- 796 neapolitanus and mortars: Comparison of the biodeterioration between Portland cement and
797 calcium aluminate cement, *International Biodeterioration & Biodegradation*. 121 (2017) 19–25.
798 <https://doi.org/10.1016/j.ibiod.2017.03.010>.
- 799 [42] M. Berthomier, C. Lors, D. Damidot, T. De Larrard, C. Guérandel, A. Bertron, Leaching of CEM
800 III paste by demineralised or mineralised water at pH 7 in relation with aluminium release in
801 drinking water network, *Cement and Concrete Research*. 143 (2021) 106399.
802 <https://doi.org/10.1016/j.cemconres.2021.106399>.
- 803 [43] R. Snellings, A. Salze, K.L. Scrivener, Use of X-ray diffraction to quantify amorphous
804 supplementary cementitious materials in anhydrous and hydrated blended cements, *Cement and*
805 *Concrete Research*. 64 (2014) 89–98. <https://doi.org/10.1016/j.cemconres.2014.06.011>.
- 806 [44] A. Beganskienė, V. Sirutkaitis, M. Kurtinaitienė, R. Juškėnas, A. Kareiva, FTIR, TEM and NMR
807 investigations of Stöber silica nanoparticles, *Mater Sci (Medžiagotyra)*. 10 (2004) 287–290.
- 808 [45] N.K. Lee, H.K. Lee, Influence of the slag content on the chloride and sulfuric acid resistances of
809 alkali-activated fly ash/slag paste, *Cement and Concrete Composites*. 72 (2016) 168–179.
810 <https://doi.org/10.1016/j.cemconcomp.2016.06.004>.
- 811 [46] A. Allahverdi, F. Škvára, Sulfuric acid attack on hardened paste of geopolymer cements Part 1.
812 Mechanism of corrosion at relatively high concentrations, *Ceramics - Silikaty*. 49 (2005) 225–229.
- 813 [47] V. Sata, A. Sathonsaowaphak, P. Chindapasirt, Resistance of lignite bottom ash geopolymer
814 mortar to sulfate and sulfuric acid attack, *Cement and Concrete Composites*. 34 (2012) 700–708.
815 <https://doi.org/10.1016/j.cemconcomp.2012.01.010>.
- 816 [48] T. Gutberlet, H. Hilbig, R.E. Beddoe, Acid attack on hydrated cement — Effect of mineral acids
817 on the degradation process, *Cement and Concrete Research*. 74 (2015) 35–43.

- 818 <https://doi.org/10.1016/j.cemconres.2015.03.011>.
- 819 [49] S. Soleimani, O.B. Isgor, B. Ormeci, Resistance of biofilm-covered mortars to microbiologically
820 influenced deterioration simulated by sulfuric acid exposure, *Cement and Concrete Research*. 53
821 (2013) 229–238. <https://doi.org/10.1016/j.cemconres.2013.06.016>.
- 822 [50] P. Sturm, G.J.G. Gluth, C. Jäger, H.J.H. Brouwers, H.-C. Kühne, Sulfuric acid resistance of one-
823 part alkali-activated mortars, *Cement and Concrete Research*. 109 (2018) 54–63.
824 <https://doi.org/10.1016/j.cemconres.2018.04.009>.
- 825 [51] M.G. Alexander, C. Fourie, Performance of sewer pipe concrete mixtures with portland and
826 calcium aluminate cements subject to mineral and biogenic acid attack, *Materials and Structures*.
827 44 (2011) 313–330. <https://doi.org/10.1617/s11527-010-9629-1>.
- 828 [52] M.P. Lavigne, A. Bertron, C. Botanch, L. Auer, G. Hernandez-Raquet, A. Cockx, J.-N. Foussard,
829 G. Escadeillas, E. Paul, Innovative approach to simulating the biodeterioration of industrial
830 cementitious products in sewer environment. Part II: Validation on CAC and BFSC linings,
831 *Cement and Concrete Research*. 79 (2016) 409–418.
832 <https://doi.org/10.1016/j.cemconres.2015.10.002>.
- 833 [53] J. Herisson, M. Guéguen-Minerbe, E.D. van Hullebusch, T. Chaussadent, Behaviour of different
834 cementitious material formulations in sewer networks, *Water Science and Technology*. 69 (2014)
835 1502–1508. <https://doi.org/10.2166/wst.2014.009>.

836